Terrestrial Photogrammetry and Numerical Modelling for the Stability Analysis of Rock Slopes in High Mountain Areas: Aiguilles Marbrées case

Curtaz M.; Ferrero A.M. ; Roncella R.; Segalini A.; Umili G.. Terrestrial Photogrammetry and Numerical Modelling for the Stability Analysis of Rock Slopes in High Mountain Areas: Aiguilles Marbrées case. ROCK MECHANICS AND ROCK ENGINEERING. 2 pp: 605-620.
DOI: 10.1007/s00603-013-0446-z

Rock Mechanics and Rock Engineering

Terrestrial photogrammetry and numerical modelling for the stability analysis of rock slopes in high mountains: the case of Aiguilles Marbrées

--Manuscript Draft--

Manuscript Number:	
Full Title:	Terrestrial photogrammetry and numerical modelling for the stability analysis of rock slopes in high mountains: the case of Aiguilles Marbrées
Article Type:	Original Paper
Keywords:	Rock fall; high mountains; remote survey techniques; stability analysis; Distinct Element Model
Corresponding Author:	Andrea Segalini, Ph.D. Università di Parma Parma, PR ITALY
Corresponding Author Secondary Information:	
Corresponding Author's Institution:	Università di Parma
Corresponding Author's Secondary Institution:	
First Author:	Michèle Curtaz, Ph.D.
First Author Secondary Information:	
Order of Authors:	Michèle Curtaz, Ph.D.
	Anna Maria Ferrero, Ph.D.
	Riccardo Roncella, Ph.D.
	Andrea Segalini, Ph.D.
	Gessica Umili, Ph.D.
Order of Authors Secondary Information:	
Abstract:	Several high altitude slope instability phenomena involving rock block of different volumes have been observed in recent years. The increase in these phenomena could be correlated with climatic variations and a general increase in temperature that induces both ice melt with consequent water seepage and glacial lowering with consequent loss of support of the rock face. The degradation of the high altitude thermal layer, which is known as "permafrost", can determine the formation of highly fractured rock slopes where instabilities can concentrate. The present research develops a methodology to improve the understanding and assessment of rock slope stability conditions in high mountain environments where access is difficult. The observed instabilities are controlled by the presence of discontinuities that can determine block detachments. Consequently, a detailed survey of the rock faces is necessary, both in terms of topography and geological structure, in order to locate the discontinuities on the slope for a better geometric reconstruction and subsequent stability analysis of the blocky rock mass. Photogrammetrical surveys performed at different times, allow the geostructure of the rock mass to be determined and for the rock block volumes and detachment mechanisms to be estimated, in order to assess stability conditions and potential triggering mechanisms. Photogrammetrical surveys facilitate both the characterisation of the rock mass and the monitoring of slope instabilities over time. The methodology has been applied in a case study, the North Face of Aiguilles Marbrées in the Mont Blanc massif, which suffers from frequent instability phenomena. A slope failure, which occurred in 2007, has been back-analysed using both, the Limit Equilibrium Method (LEM) and 3D Distinct Element Modelling (DEM). The method has been supported and validated with traditional in situ surveys and measurements of the discontinuity orientation and other rock mass features.

Terrestrial photogrammetry and numerical modelling for the stability analysis of rock slopes in high mountains: the case of Aiguilles Marbrées

Authors:

M. Curtaz*, A.M. Ferrero***, R. Roncella**, A. Segalini**, G. Umili**

Affiliations:

- * Fondazione Montagna sicura

loc. Villard de la Palud 1
11013 Courmayeur (AO)
Italy
Fax 00390165897647

- ** University of Parma

Department of Civil, Environmental and Territory Engineering (DICATeA)
Vl. Usberti 181/a
43124 Parma
Italy
Fax 00390521905924

- *** University of Turin

Department of Earth science
Via Valperga Caluso 35
10100 Torino
Italy
Fax 00390521905924
annm.ferrero@unito.it

ABSTRACT

Several high altitude slope instability phenomena involving rock block of different volumes have been observed in recent years. The increase in these phenomena could be correlated with climatic variations and a general increase in temperature that induces both ice melt with consequent water seepage and glacial lowering with consequent loss of support of the rock face. The degradation of the high altitude thermal layer, which is known as "permafrost", can determine the formation of highly fractured rock slopes where instabilities can concentrate.

The present research develops a methodology to improve the understanding and assessment of rock slope stability conditions in high mountain environments where access is difficult. The observed instabilities are controlled by the presence of discontinuities that can determine block detachments. Consequently, a detailed survey of the rock faces is necessary, both in terms of topography and geological structure, in order to locate the discontinuities on the slope for a better geometric reconstruction and subsequent stability analysis of the blocky rock mass. Photogrammetrical surveys performed at different times, allow the geostructure of the rock mass to be determined and for the rock block volumes and detachment mechanisms to be estimated, in order to assess stability conditions and

potential triggering mechanisms. Photogrammetrical surveys facilitate both the characterisation of the rock mass and the monitoring of slope instabilities over time.

The methodology has been applied in a case study, the North Face of Aiguilles Marbrées in the Mont Blanc massif, which suffers from frequent instability phenomena. A slope failure, which occurred in 2007, has been back-analysed using both, the Limit Equilibrium Method (LEM) and 3D Distinct Element Modelling (DEM). The method has been supported and validated with traditional in situ surveys and measurements of the discontinuity orientation and other rock mass features.

Keywords: Rock fall, high mountains, remote survey techniques, stability analysis, Distinct Element Model

INTRODUCTION

The general global climatic scenario indicates a rise in temperatures, particularly in the northern hemisphere and in the alpine area, where the temperature increase is higher (1.5 °C) (Ravanel and Deline, 2011) than that registered on the global scale (0.74 °C) between 1906 and 2005 (IPCC, 2007).

Suter (2002) and Vincent et al. (2007), show that the response to atmospheric warming is amplified in glacier ice, which makes the effects of climate change even more evident.

During the last few years a considerable number of rock falls, debris flows and avalanches involving large volumes of rock, snow and ice, have been observed at altitudes above 3000 m a.s.l. of which: Brenva, 1997 (Barla et al., 2000); Grandes Jorasses, 2007; Matterhorn 2003; Punta Thurwieser 2004; Drus 2005 are representative examples in the Western Alps area. Most of these events occurred during periods that were characterised by the specific climatic situation of thermal zero above 3000 m a.s.l. for many consecutive days, which suggests a possible link between climatic conditions and rock falls (Dutto and Mortara, 1991; Dramis et al., 1995; Deline, 2001; Haeberli et al., 2003; Noetzli et al., 2003 Gruber and Haeberli, 2007). This link appears to be connected in particular to the degradation of the high altitude thermal layer, known as "permafrost" (characterised by temperatures of less than zero for a continuous period of at least 2 years, Allen et al., 2009).

Ravanel and Deline (2011) have documented the described phenomena and presented an inventory of rock falls that have occurred since the end of the 'Little Ice Age' on the north side of the Aiguilles de Chamonix (Mont Blanc massif). They have also shown how rock fall phenomena occur more frequently during warm summers, as in the case of 2003 and how they are concentrated on slopes with average elevations (3130 m a.s.l.) close to the lower modelled permafrost limits. A similar inventory has been made for the Aosta Valley, in which events that occurred in high mountain regions have been

collated by alpine guides. The work, which began in 2006 with UE founding, involved France and Switzerland (CENSI CRO) (Figure 1) and revealed results that are in agreement with Ravanel and Deline's (2011) data.

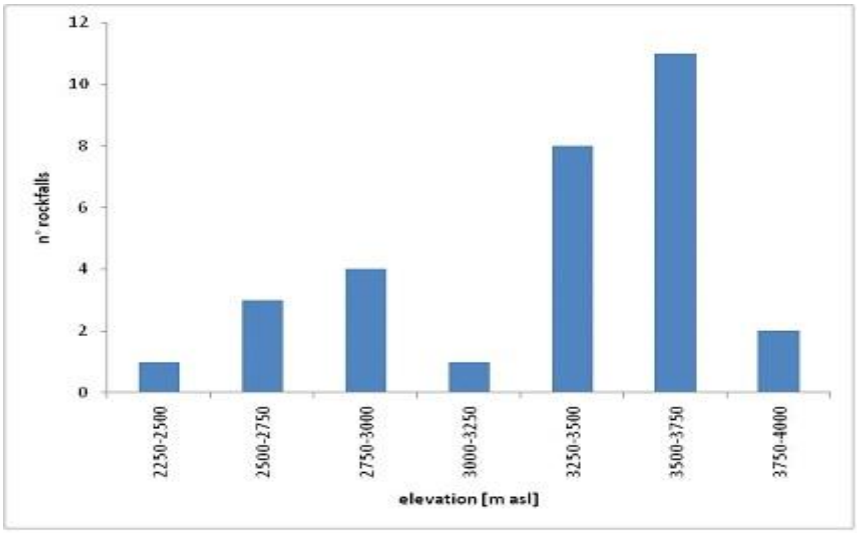

Figure 1. Rock fall events recorded in the Aosta Valley (Italy) between 2006 and 2009 (CENSI_CRO final report, 2009).

Slope stability is connected to ice melt and the consequent water seepage in the rock mass's fracture network or in soil deposits. Seepage determines the degree of saturation with different kinds of resulting effects; an increase in water pressure due to the increased water level but additionally, further pressures due to changes of water phase when the temperature subsequently decreases, which determines water freezing. Moreover, thawing can reduce the strength of soil and rock and can destabilise slopes leading to failure (Huggel, 2009).

In the case of rock masses, the formation of ice in confined situations can induce high pressure due to increases in volume. The discontinuity persistence is often below 100% and rock bridges have a remarkable influence on the stability evolution of rock blocks. Rock bridge failure, induced by water/ice pressure, determines progressive failure that can be monitored over time. Rock fracture propagation due to ice segregation growth in water saturated rocks with interconnected cracks shows considerable damage (Hallet et al., 1991). Both rock mass structure and climatic conditions determine the instability phenomena, whereas the freeze-thaw penetration controls the maximum dimension of detachable blocks and joint spacing on the rock face affects the size distribution of rock fall debris (Matsouka and Sakai, 1999).

In situ monitoring and laboratory testing could help to improve the understanding of these complex phenomena. However, the difficult operational environments at high elevations due to severe logistical and climatic conditions often determine some limitation to the data that can be acquired (Matsouka and Sakai, 1999). Non-contact methods based on photogrammetry, which are able to provide information on the rock mass structure and topography (Harrison and Reid, 2000; Kemeny et al., 2003; Jaboyedoff

et al., 2009; Ferrero et al., 2011a; Ferrero et al., 2011b; Sturzenegger and Stead 2009a; 2009b; Gigli and Casagli, 2011) and thus, give information on the slope structure and on its hydrogeological conditions, are particularly appropriate for this environment, where standard methodologies are often not applicable (Hallet et al., 1991).

The rock fall that occurred in September 2007 in the lower part of the Aiguilles Marbrées has been studied by the authors. To establish a working methodology for the analysis of this kind of phenomenon is the main subject of this paper. The 3600 m^3 rock volume that detached from the rock wall was well defined by fractures that were visible before the movement. An ice layer was still visible for days after the collapse in the rockfall scar and along the sliding surface; this is the reason why a possible relationship to permafrost degradation was considered as the cause of the fall, rather than a decrease in stress caused by glacier shrinkage.

FIELD SURVEY

GEOLOGICAL AND GEOSTRUCTURAL SETTING

Aiguilles Marbrées is a granitic peak 3535 m a.s.l. that is part of the Mont Blanc massif. The study area is located in the lower portion of the North face (geographical coordinates WGS84 45° 51' 8.19" N, 6° 56' 23.15" E), which is characterised by a mean gradient and orientation of about 70° and 320° N, respectively.

From a structural and geomechanical point of view, Aiguilles Marbrées can be separated into three principal domains (Figure 2). The results presented in this paper are based on the analysis of domain 3, where instabilities concentrate but can be applied to the whole slope because it shows a similar rock mass structure. Therefore, this study could easily be extended to the entire Aiguilles Marbrées in the future.

Figure 2. The Aiguilles Marbrées N and W faces.

Surveys have shown that the rock walls are characterised by steep slopes with an elevation difference from the base of the glacier to the slope peak that varies between 50 and 100 m. These walls are composed of an alternation of flat surfaces (with disjointed rock) separated by peaks and needles. The entire rock mass is heavily fractured. The main discontinuity set is steeply dipping towards the north (340°/65°).

Domain 3 is the one that is most frequently affected by moderate rockfalls (typical average volume: 20–25 m^3), even though all the domains are characterised by a similar rock mass structure; the failure mechanism is due to shearing movements along sub-vertical fractures,

The fall that occurred in September 2007 can be delimited by fractures that were visible before the movement. The failed mass was geometrically composed of two overlapping parallelepiped rock slabs, the larger of which rested on top of the smaller, separated by a discontinuity plane roughly parallel to the slope face. From the available information, it was not possible to discern how the kinematic mechanism evolved (either the larger slab first and then the other, or both at the same time). Hence, in the analyses described herein, it was presumed that the slab failures occurred simultaneously, as if the two slabs were a single rock block (Figure 3). The observation of the rock surfaces exposed after the failure indicated the presence of rock bridges that had broken just before the rock fall. In other words,

the main hypothesis on the failure mechanism evolution implies that the presence of rock bridges guaranteed the rock block stability observed before the event.

Figure 3. Observed instability phenomena. Comparison between photos taken on August 7, 2007 and September 24, 2007. The exact dates of rockfalls are unknown. Total dotted area is about 60 m high, 15 m wide and 4 m deep.

The closest climatic data were collected at Punta Helbronner meteorological station (3462 m a.s.l.). They showed, for the period August 7 to September 24 (70 days), a total of 32 days on which the minimum temperature was above 0 °C. It is also possible to observe a cycle with the highest variation (from 7 °C to -8 °C) among all the cycles.

Since 2009, rock temperature data have been collected at the same meteorological station using a sensor located 55 cm below the rock surface. The observed annual trends (2009-2010-2011) of rock temperature show that between the beginning of June and the end of September the average temperature is above 0 °C (Figure 4). Since 2007, the air temperature trend has been very similar to that observed in 2010, particularly starting from September 10th and thus, we consider that the 2007 rock temperature data would be similar to those recorded in 2010. In Figure 5, it is possible to observe a decreasing trend of the rock temperature towards 0 °C with less frequent and less marked fluctuations than those observed in the air temperature trend but still connected to it. A sudden decrease in the air temperature (between the 27th and 30th of August) resulted in a rock temperature below 0 °C for 1 day. A similar phenomenon could have occurred corresponding to the 2007 temperature decrease (recorded between August 27 and September 5) with an estimated rock temperature falling below 0 °C for a few days and then increasing again.

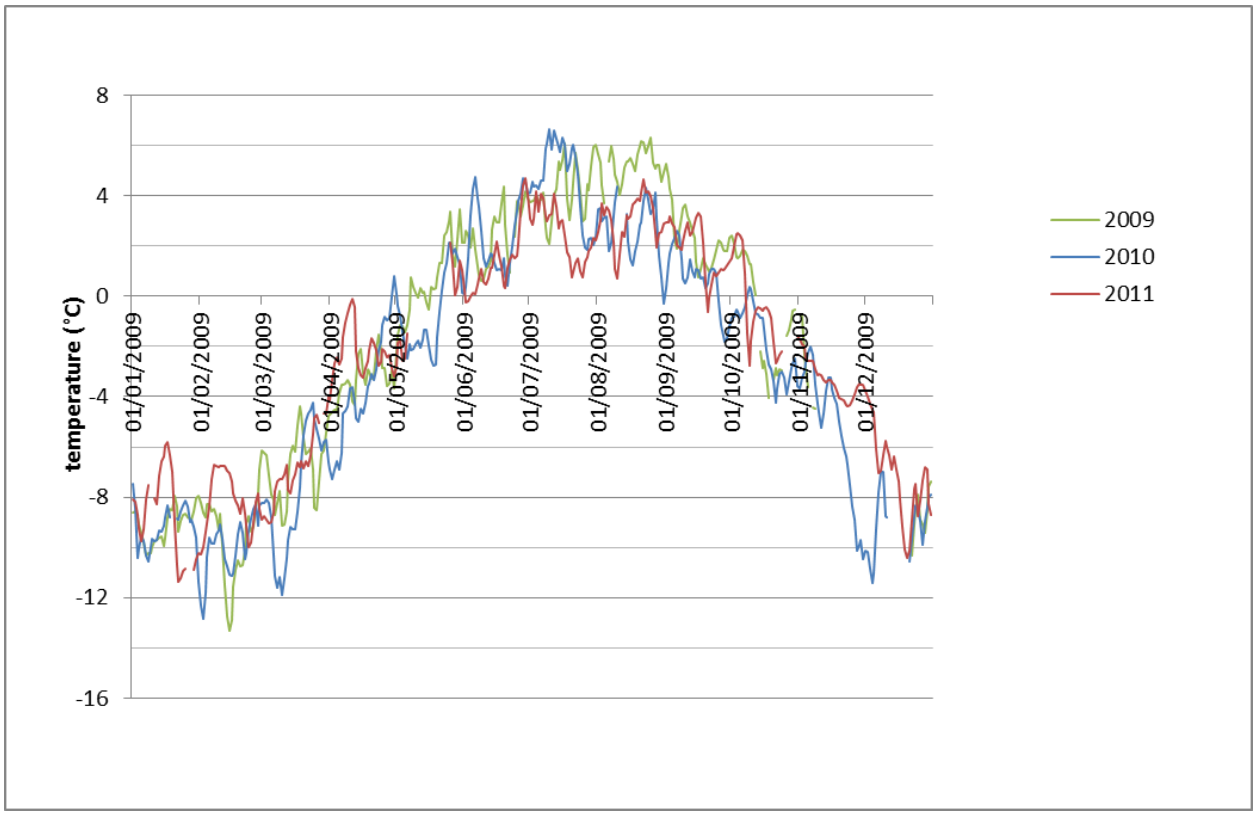

Figure 4. Rock temperature data collected at Punta Helbronner meteorological station.

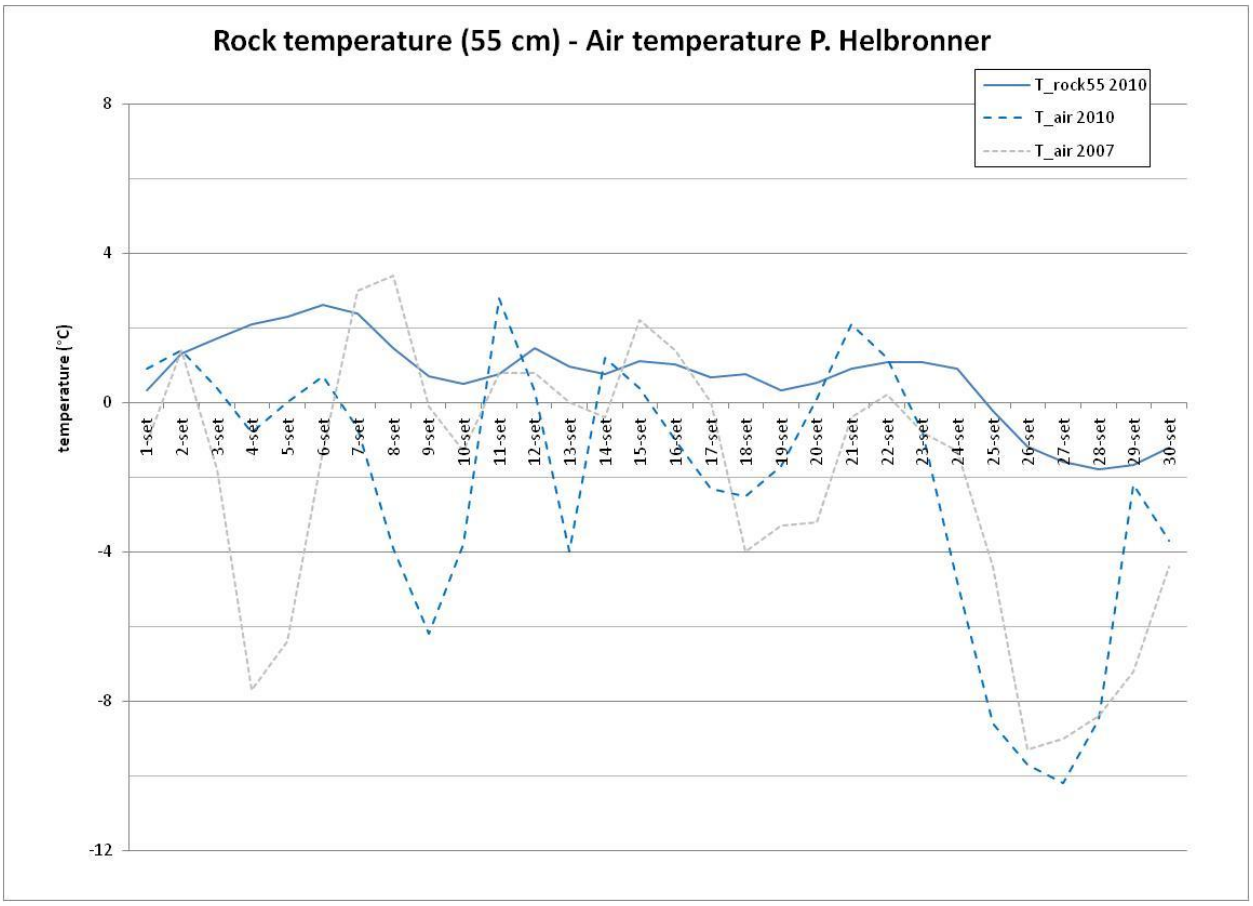

Figure 5. Comparison between rock and air temperature data.

PHOTOGRAMMETRIC SURVEY

Periodic photogrammetric surveys were conducted during the spring and summer months of 2008 (five monthly surveys from April to September 2008) and 2009 (five monthly surveys from May to October 2009) on the North Face of Aiguilles Marbrées using a Nikon D700 digital camera with a calibrated 20 mm focal lens. A traditional topographic survey of ground control points on the rock surface was not feasible and therefore, in the first survey (April 2008), the camera was coupled to a GPS antenna/receiver through a calibrated pole in order to determine the orientation parameters of the images block. The technique (also known as *photo-GPS* technique) was first developed and tested by Forlani and Pinto (2007). The GPS records the antenna position for each image in a world coordinate reference system (WGS84); because its position is fixed in the image reference system (by means of the calibrated pole) a constrained bundle-adjustment, which imposes that the camera centre has a fixed relative position with respect to the antenna, can be calculated. At the end of the processing, both the camera centre coordinates and the camera pose (rotation of the camera) are estimated in the world coordinate reference system. In this first Aiguilles Marbrées survey, the ground control points were measured using this technique and then used in the subsequent surveys, as well. Due to the rather long base-length between the GPS receiver and the base station, an absolute planar accuracy in the range of 2–6 cm can be estimated. Nevertheless, the relative accuracy between the subsequent camera positions in the block adjustment is certainly higher (1–3 cm) and this leads to a final precision on the control points of between 1.5 cm (for the nearest points, located at about 55 m from the camera) and 7 cm (for the furthest ones, located at about 140 m from the camera).

All the image sequences were automatically processed to accelerate the block orientation step using structure and motion algorithms developed by Roncella et al. (2005).

Finally, a high resolution (approximately 100 pts/m^2) DSM of the rock wall was obtained, using dense matching routines (Roncella, 2005) based on Least Squares Matching (LSM) (Grün, 1985) and Multi-photo Geometrically Constrained Matching (MGCM) (Grün and Baltsavias, 1988) algorithms.

The main advantage of a digital model is that it is possible to work on it without a time limit and to measure and process data whenever it is necessary. Traditional surveys would require the operator to return to the site with all the inconvenience in terms of time, costs and operational safety. Moreover, using this technique, it is possible to study parts of the slope that are difficult or even impossible to

reach by an operator. The slope dimensions and mobilised volumes can be measured from the DSM

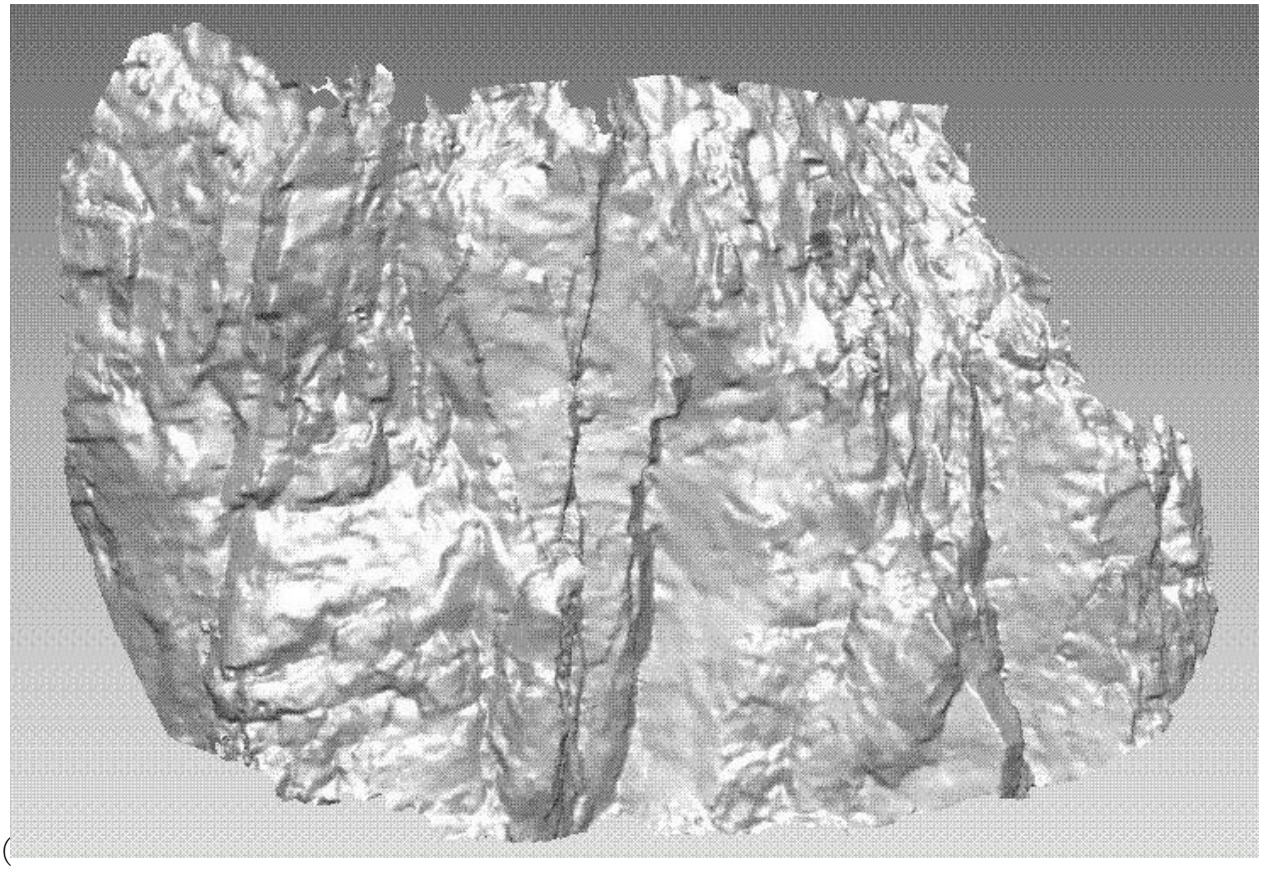

(Figure 6); furthermore, the rock fall activity can be monitored from a comparison of the DSMs at different times and the mobilised volumes can be determined from the differences between the diachronic models. A comparison of the DSMs at different times (June 2009 – October 2008) is shown in Figure 7a and outlined in the photograph of Figure 7b, where the 2007 phenomenon area is also delimited. The first survey served many purposes; apart from the photogrammetric block orientation, its model was used as a baseline to compare the subsequent surveys and to detect possible collapses.

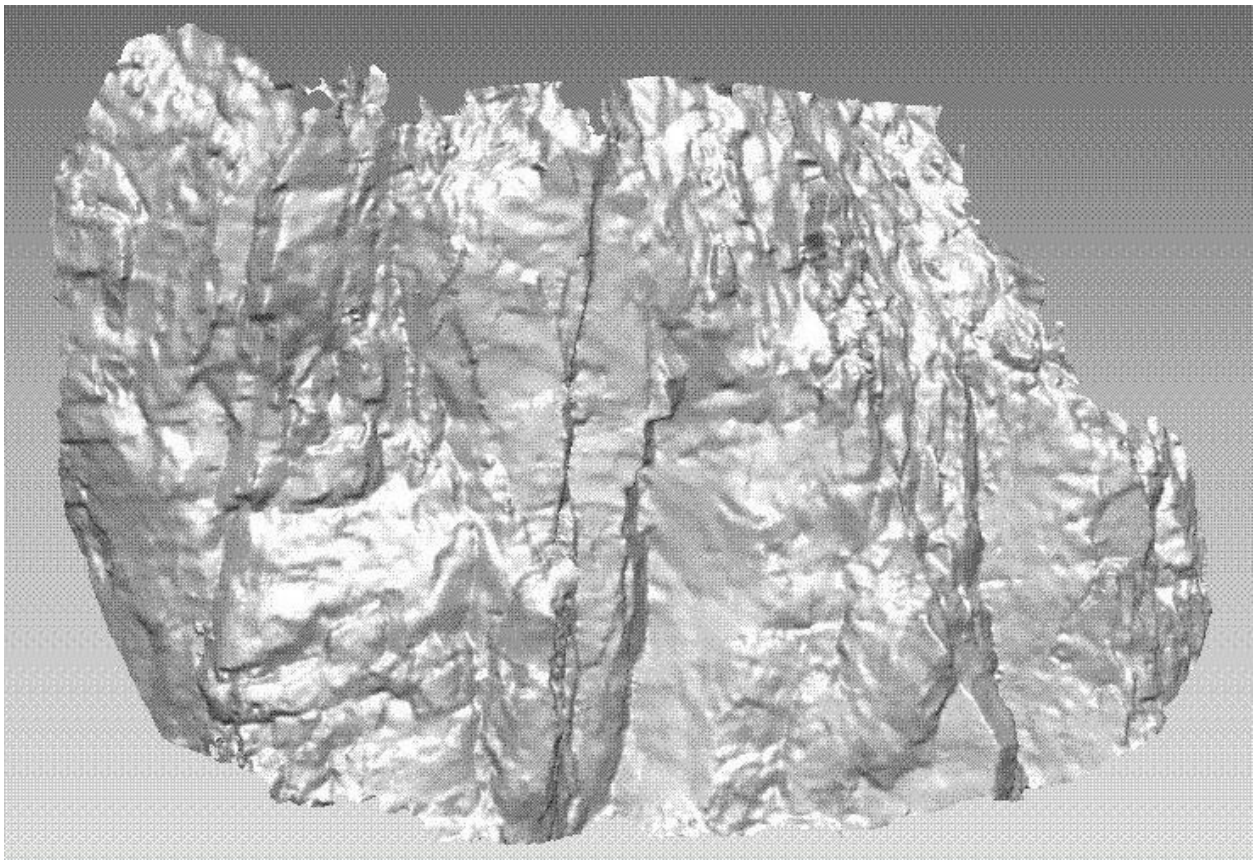

Figure 6. DSM image of the North Face of the Aiguilles Marbrèes (domain 3). [TIN model composed by 226093 points; base 85 m, height 60 m]

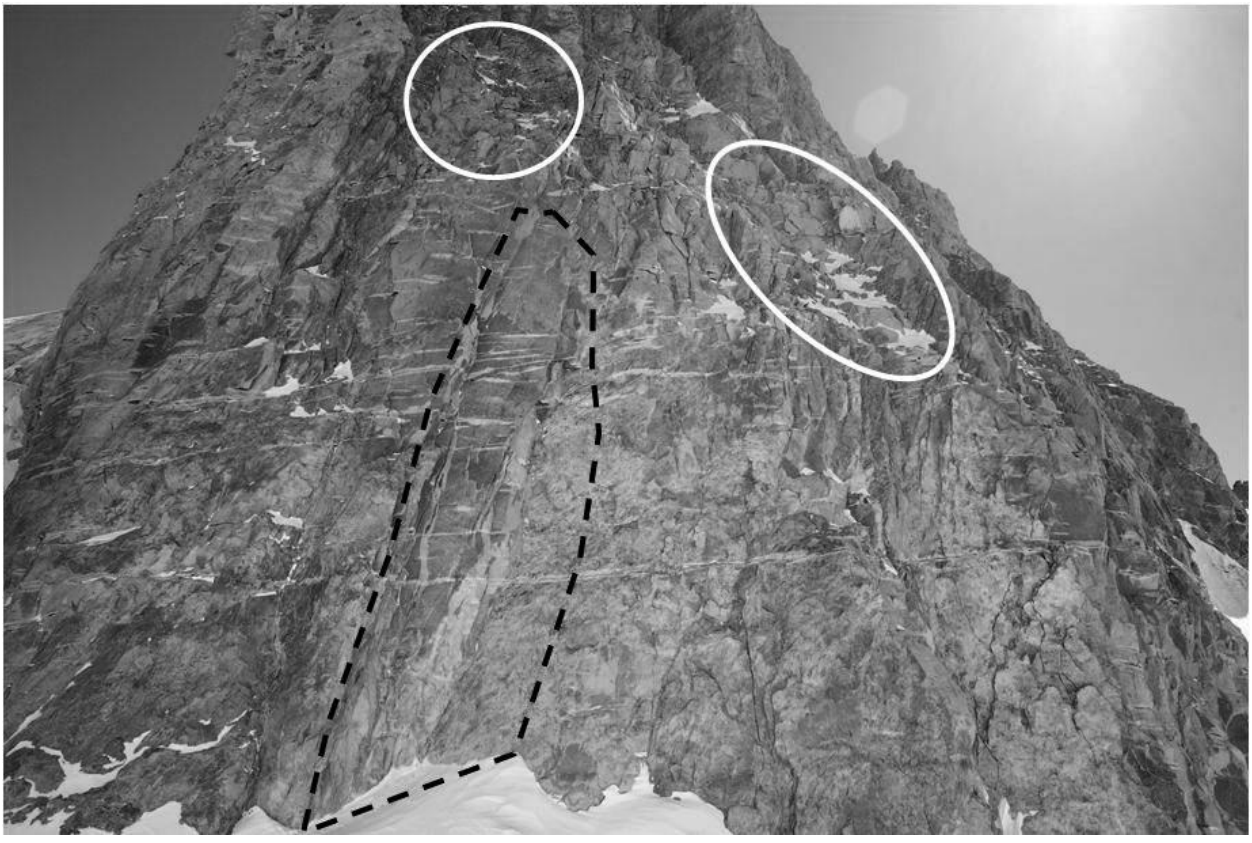

Figure 7. Comparison between the DSMs at different times and identification of the differences (7a). In Figure 7b the same areas are evidenced in a photo where: white areas indicates places of snow accumulation; 2007 phenomenon area is delimited in black.

As the distance of the object with respect to the subsequent camera positions is relatively low (between 55 and 80 m), at least for the area considered in the production of the DSM and assuming a point restitution accuracy of between 1.5 and 3 cm (evaluated through variance propagation in the least squares bundle adjustment), any difference higher than 6–8 cm between the DSMs acquired at different times should be considered significant from a statistical point of view. The model outlines the zones of geometrical differences that are in good agreement with the in situ observations, as shown in Figure 7, which indicates the presences of snow accumulation.

The Rockscan software (Roncella et al., 2005) can perform a detailed structural survey by combining photographs taken during the photogrammetric survey and a DSM; it allows the discontinuity planes on the photographs to be recognised and simultaneously, their positions and orientation (dip and dip direction) to be defined. The operator delimits discontinuity planes manually on a photograph; because exterior and interior orientation parameters are given for each photograph, the point cloud (or the DSM) can be projected onto the chosen photo. The software then calculates the plane that best fits the points contained in the region on the image delimited by the operator. This method allows a large number of planes to be defined quickly and the examined slope structure can be studied using a larger statistical sample than that which could be obtained using data sampled along a few scanlines on the rock face. The global view of the rock mass on the image makes the definition of the principal discontinuity sets straightforewardand more complete than the limited view that the operators have during a traditional survey. Determining easily recognised discontinuity planes at this stage makes the identification of outliers (i.e., points not lying on the plane) more simple and the computation of the dip and dip direction faster.

In this study, four photographs were used to obtain a representative sample of the rock mass discontinuity sets. A total of 441 discontinuity planes were identified. The dip and dip direction were

calculated for each plane using the Rockscan software

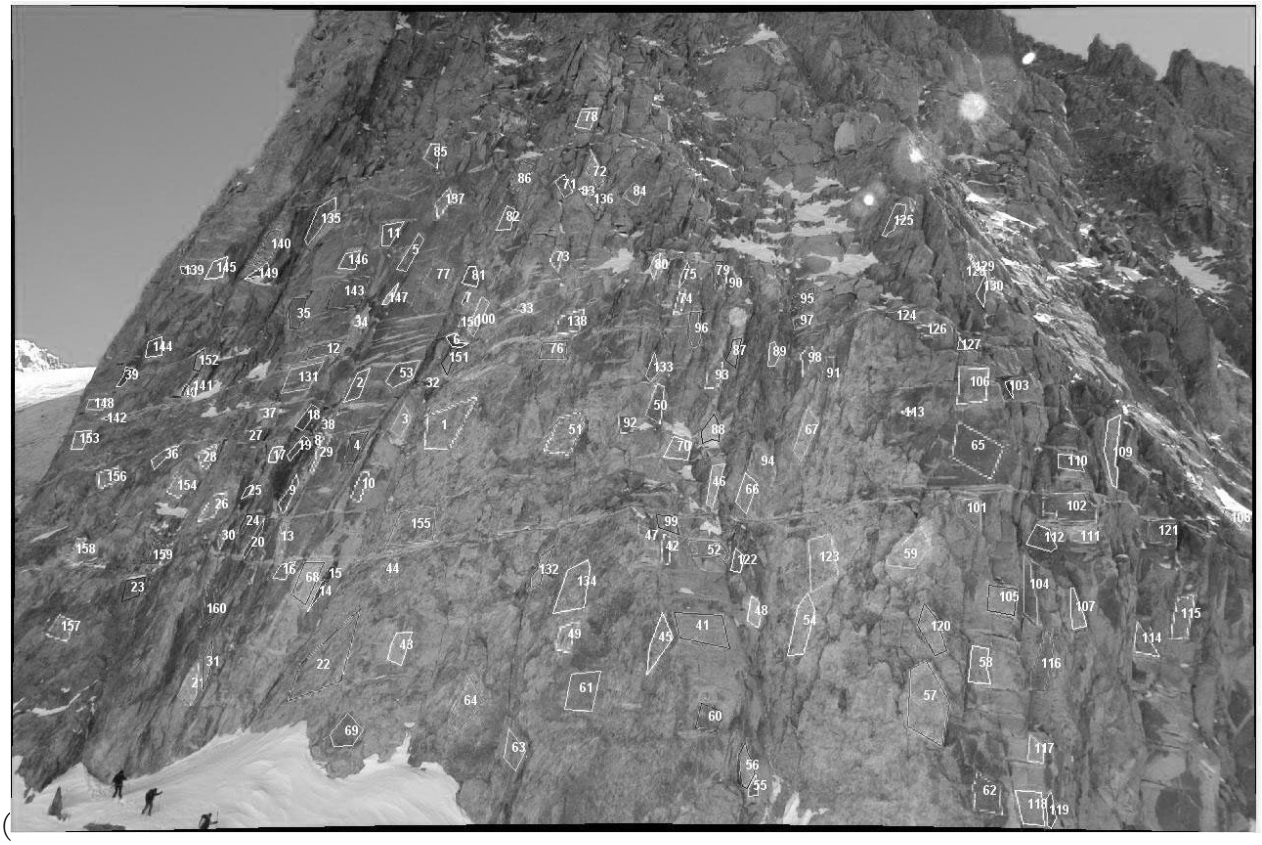

(Figure 8).

The analysis highlighted that the sub-horizontal discontinuity sets were difficult to recognise; the fractures were often closed, except in the case of roofs created by rock collapses. This photogrammetric survey only takes frontal views and therefore, these roofs cannot be delimited. Occlusions and low view angles reduce the number of points sampled in these areas and the solution (proposed, for example, in Sturzenegger and Stead, 2009b) is to survey the outcrop from different positions, although in this case it was not possible due to the obvious movement limitations.

Figure 8. Discontinuity planes delimited manually on a photograph.

DATA PROCESSING

The orientation data of all the discontinuities were processed with the DIPS® (Rocscience, 2009) software, which permits a stereographic projection of poles and the identification of discontinuity clusters. These can be contoured and discontinuity sets identified. The pole distributions may be biased because of the difficulty involved in resolving certain plane orientations (i.e., sub-horizontal sets). By projecting all of the 441 sampled planes onto a concentration stereogram, four principal discontinuity sets (ID 1m, 2m, 3m and 4m) can be identified (Figure 9).

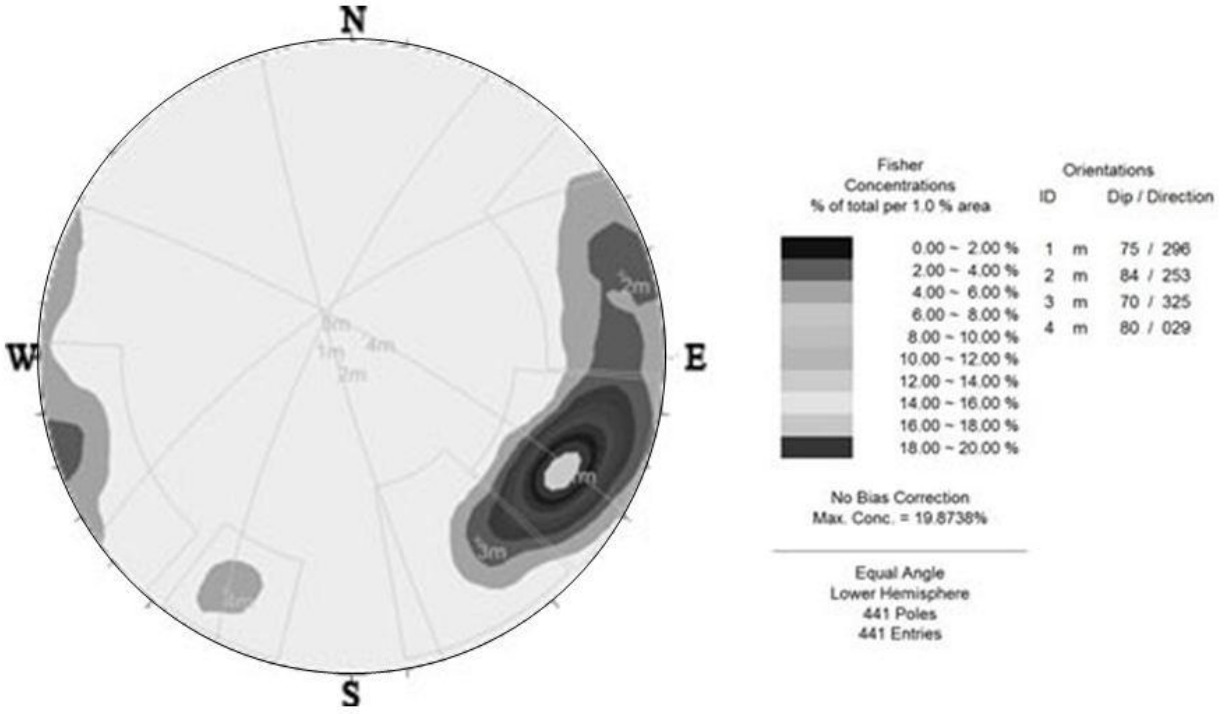

Figure 9. Contoured stereonet of the planes identified using the Rockscan software.

It is important to notice that only sets with a certain number of poles emerge from the contoured stereonet and therefore, sub-horizontal sets are absent because only a few planes were delimited, as previously explained. Consequently, it is necessary to carefully analyse the stereonets in which the poles of that set are visible (ID 5m in Figure 10).

This is a typical situation of a poorly represented set because of a bias error due to the logistical impossibility to shoot photographs in points well distributed along the vertical dimension of the slope. These kinds of shots would have required an aerial survey that was not available. In this case, aware of the possible lack of data, special care was given to define the sub-horizontal set. Discontinuity traces and rock mass fracture analysis was carried and more details are given in Ferrero and Umili (2011) and in Umili et al. (2012).

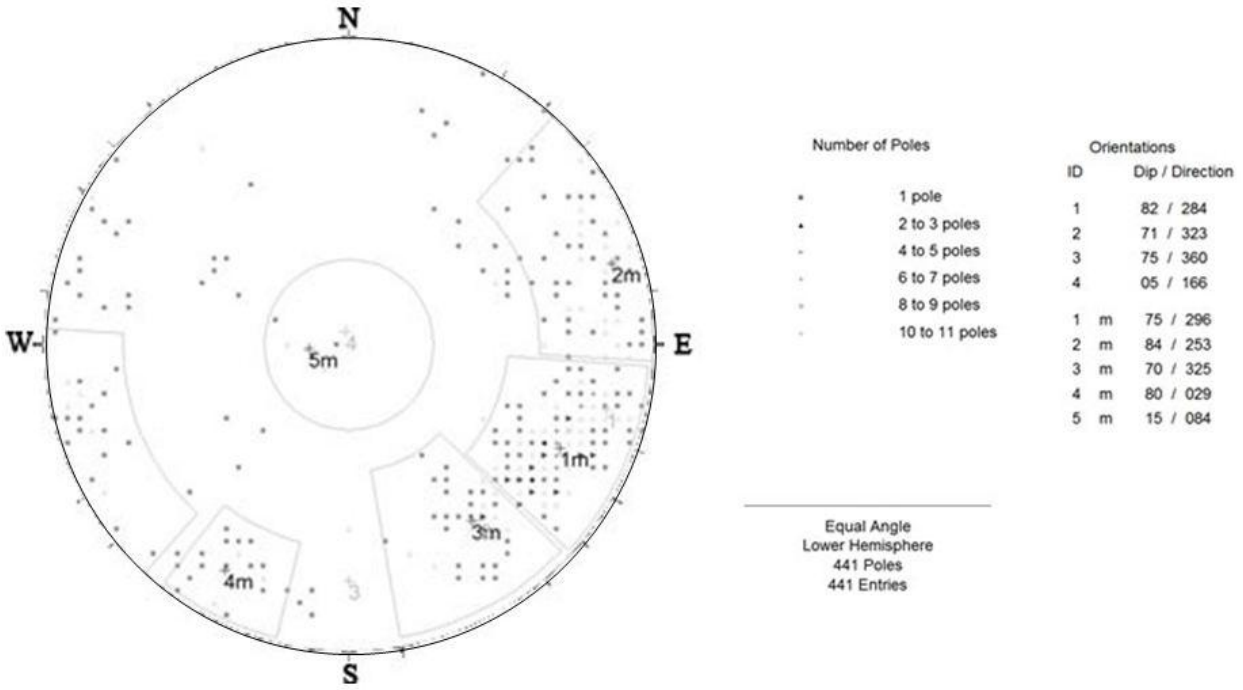

Figure 10. Discontinuity stereonet of the poles identified using the Rockscan.

COMPARISON WITH THE TRADITIONAL SURVEY

A traditional survey was carried out in order to verify the data obtained using Rockscan. This survey was conducted along two different lines of about 25 m in the lower part of the rock face, on the right and left sides of the central portion of the slope, where the rock fall occurred in 2007. The dip and dip direction of the rock planes were measured using a geological compass. A total of 62 orientation data were collected and processed with the DIPS® software. The rock strength values were estimated using a Schimdt hammer and the roughness profiles were measured during the field survey adopting a standard Barton profilometer.

A good correlation was found between the Rockscan results and those obtained from the traditional survey (Table 1); i.e., the same main rock plane families were found. Evidently, there were some gaps but they can be considered acceptable because the obtained set orientations were mean value data clouds that showed a certain dispersion and because the aim of the analysis was to define the general structure of the rock mass and the main kinematic mechanisms.

Table 1. Mean orientation values and differences obtained with Rockscan and with the traditional survey. The ID discontinuity set is shown in parentheses.

Discontinuity set	**Traditional survey**	**Rockscan survey**	**Differences**
Parallel to the cliff face	82/284 (1)	75/296 (1m)	7 / 12
Lateral release	75/000 (3)	80/029 (4m)	5 / 29
Sub-horizontal	05/166 (4)	15/084 (5m)	10 / 82
Other	71/323 (2)	70/325 (3m)	1 / 2

The set parallel to the cliff face (ID 1/1m), which creates the detachment and sliding surface of the rock volume that fell in September 2007, dips in a W/NW direction in both surveys. There was good agreement for the sub-vertical set (ID 3/4m), which isolates the rock slabs laterally; this set was perpendicular to the previous one. The values concerning the sub-horizontal set show the largest differences between the two surveys. It should be pointed out that it is more difficult to determine the dip direction for a sub-horizontal set; moreover, the measurements carried out successfully with Rockscan are few and scattered. In this case, the traditional survey value could be more reliable.

As shown in Figure 11, the sub-horizontal set (ID 5m) creates roofs and the sub-vertical set (ID 4m) isolates rock slabs laterally; slab sliding occurs on the set parallel to the fall (ID 1m).

Figure 11. Identification of the rock fall phenomena. The sub-horizontal set (ID 5m) creates roofs and the sub-vertical set (ID 4m) isolates rock slabs laterally; slab sliding occurs on the set parallel to the fall (ID 1m).

Virtual scan lines were also traced on the orthophotograph of the rock face and this allowed the spacing of the joint set to be determined, which turned out to be 2.7 m ± 1 m for joint set 1 and 3.1 m ± 2 m for joint set 5.

ANALYSIS OF THE STABILITY CONDITIONS

THE LIMIT EQUILIBRIUM METHOD

At first, a back-analysis was performed using the limit equilibrium method (Ferrero et al., 2010). The problem was simplified in order to analyse the influence of rock bridges/fracture persistence on the surface along which the sliding had occurred, as well as the influence of pore pressure due to the presence of water coming from ice melt.

The possible presence of ice adhesion was conservatively neglected. The mechanical behaviour, in terms of stiffness and strength of an ice-filled joint, is a function of both normal stress and temperature (Davies et al., 2001; Günzel, 2009). Günzel observed that in constant stress tests, ice-filled joints show a parabolic relationship between normal stress and shear stress and a maximum peak of resistance is observed for a normal stress of between 300 and 400 kPa for both examined temperatures. However, the parabolic relation tends towards a very low intersection with the y-axis and consequently, to a very low cohesion value. Davies et al. (2001) proposed a linear shear strength envelope for ice-filled joints, extrapolating experimental data down to zero normal stress, although their experimental data were starting for a confined stress of 100 kPa. In the Aiguilles Marbrées case, the normal stresses acting on the failure joint are very low due to the inclination and shallowness of the sliding blocks and therefore, operate in a range of values where too little experimental evidence is available to allow for a safe assumption regarding ice adhesion strength.

Moreover, the physical mechanisms responsible for ice adhesion are due to the electrostatic interaction of molecules and are functions of the electrical property of the surface of ice and ice adhesion (Ryzhkin and Petrenko, 1997), which has not been experimentally or theoretically evaluated for rough rock joints. These considerations have led the authors to neglect the possible contribution of ice adhesion to the shear strength and to consider that it would be much less significant than the contribution of rock bridges.

Murton et al. (2001) have performed some interesting tests on moist chalk that was maintained at sub-zero temperatures while the upper half was cyclically frozen and thawed, simulating seasonal temperature cycles in an active layer. They observed that the material located above the permafrost limit became “strongly brecciated and rich in segregated ice”. However, this kind of phenomenon does not apply to granite, because granite has a much lower porosity in comparison with chalk, which does not allowing ice segregation. Moreover, no rock brecciating can be observed in situ in such a rock type. Consequently, the different scenarios investigated in this paper were translated into the acting and resisting forces shown in Figure 12. Before the collapse, the discontinuity trace that isolated the block from the overhanging face was visible; therefore, the force called A in Figure 12, which represents the rock tensile strength at the slab top, is absent.

The block was free on the right-hand side (observing the rock face from the front), while there was a visible discontinuity trace on the left-hand side. As it is impossible to calculate the perpendicular component of the force exchanged between the two fracture edges, it is impossible to assign a value to the sliding resistant component B given by the fracture surface. Therefore, B was omitted as well, which is a conservative assumption.

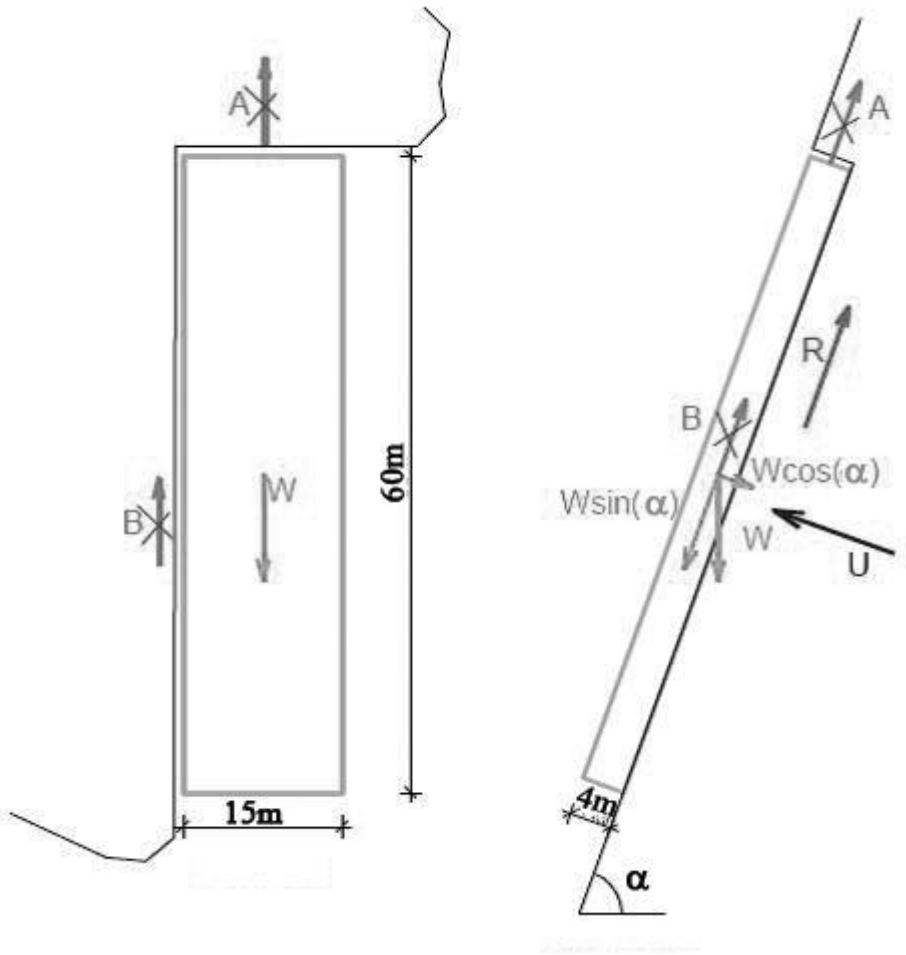

Figure 12. Force diagram on unstable block: a) front view; b) vertical section.

Therefore, the only contact surface between the volume and the surrounding rock was represented by the surface S below the slab (width 15 m, height 60 m), along which the sliding occurred.

The forces involved are:
W : weight , W = γ* volume;
R : force given by friction along discontinuity surface S, which is resistant to rock sliding;
U : hydraulic pore pressure, which depends on the height of the water column inside the fracture.

The analysis was performed assuming that the collapse had been caused by an imbalance between sliding and resistant forces. Different hypotheses concerning resistant force R were examined, in relation to the assumed discontinuity parameters (in particular the persistence).

Discontinuity strength parameters were obtained with the RocData® 4.0 code (Rocscience, 2007), which applies the Barton-Bandis (Barton, 1972) failure criterion (Table 3). The discontinuity roughness coefficient (JRC = 12) and joint compressive strength (JCS = 100) were measured in situ and used to calculate the joint strength. The base friction angle was taken from literature data for similar lithology (Giani, 1992) and was equal to 30°. The Barton-Bandis criterion was linearised considering a slope height of 60 m and a friction angle of 35° was determined. Table 3 also reports rock matrix parameters for rock bridges from Giani (1992).

An assumed intact, uniaxial compressive strength equal to 250 MPa is taken for granite. The Hoek-Brown failure criterion (2002) was assumed and the consequent parameters determined as follows: disturbance factor D was assumed to be 0 because no excavations or explosions had occurred on the slope; s = 1 and a = 0.5 for intact rock; m_i is equal 32 for granite; and the intact rock Young's modulus E_i was calculated to be 106 GPa, considering relationships from Palmstrom and Singh (2001).

Therefore, the system of forces acting on the rock block is composed of sliding and resisting forces that can be determined as follows:

Sliding Forces: $W \cdot \sin\alpha$

Resistant Forces: $\left[W \cdot \cos\alpha - U\right] \cdot \tan\phi + c \cdot S_{rockbridge}$

The condition in which sliding occurs is: *Sliding Forces* > *Resistant Forces* and the corresponding Safety Factor is $SF = \dfrac{\text{Sliding Forces}}{\text{Resistant Forces}}$

Considering the resistance criterion and parameters listed in Tables 2 and 3, it is possible to conduct parametric analyses.

$$\tau = k \cdot \left(c_j + \sigma \cdot \tan\varphi_j\right) + \left(1-k\right) \cdot \left(c_r + \sigma \cdot \tan\varphi_r\right)$$

where the joint continuity k is $k = L_j / \left(L_j + L_r\right)$, L_j is the joint length, L_r is the rock bridge length and τ is the resisting stress.

Table 2: Geometry.

L_a	Block dimension	15 m
L_b	Block dimension	60 m
L_c	Block dimension	4 m
V	Block volume	3600 m^3
$S = L_a \cdot L_b$	Sliding surface	900 m^2
□	Sliding surface angle	80 °

Table 3: Rock bridge and joint parameters.

γ	Specific weight	2.7 kg/dm^3
φ_j	Joint friction angle	35 °
c_j	Joint cohesion	0 MPa
φ_r	Rock bridge friction angle	46 °
c_r	Rock bridge cohesion	25 MPa

The persistence was considered as the ratio between the joint and the rock bridges lengths and the analysis condition was taken as a slope of infinite length. This assumption was made in order perform a generalised parametric analysis of the influence of persistence, joint inclination and the water level on the safety factor of the slope. However, the chosen hypothesis can be considered representative of the real conditions because the field survey on the Aiguilles Marbrées identified the presence of several potential long sliding planes.

The results are reported in Figures 13, 14 and 15. It can be seen that when the hydraulic pressure is absent and a cohesion value of 25 MPa is assumed, even the smallest percentage of rock bridges (1%) is sufficient to ensure block stability. By reducing the cohesion value while keeping the other parameters constant, one can observe that the system is stable until the cohesion value reaches 9 MPa, which is very low for granite. Joint cohesion should be considered as a percentage contribution of the real discontinuity persistence. In other words, the rock bridge contribution to the shear strength of each joint can be considered as an increase in the cohesion value proportionate to the single joint persistence. This hypothesis implies that the rock bridges resistance is spread over all the discontinuities. Zero persistence would be represented by a cohesion equal to the intact rock strength, whilst a persistence of 100% would result in a value of zero cohesion. Taking a more realistic cohesion value of 25 MPa (computed considering an estimated joint persistence) as constant, the water column height (and therefore the hydraulic pressure) was varied to study its influence on the stability. Sliding occurs when the water column in the joint becomes higher than 13 m (which is equivalent to a force of 84.5 MN with a triangular distribution).

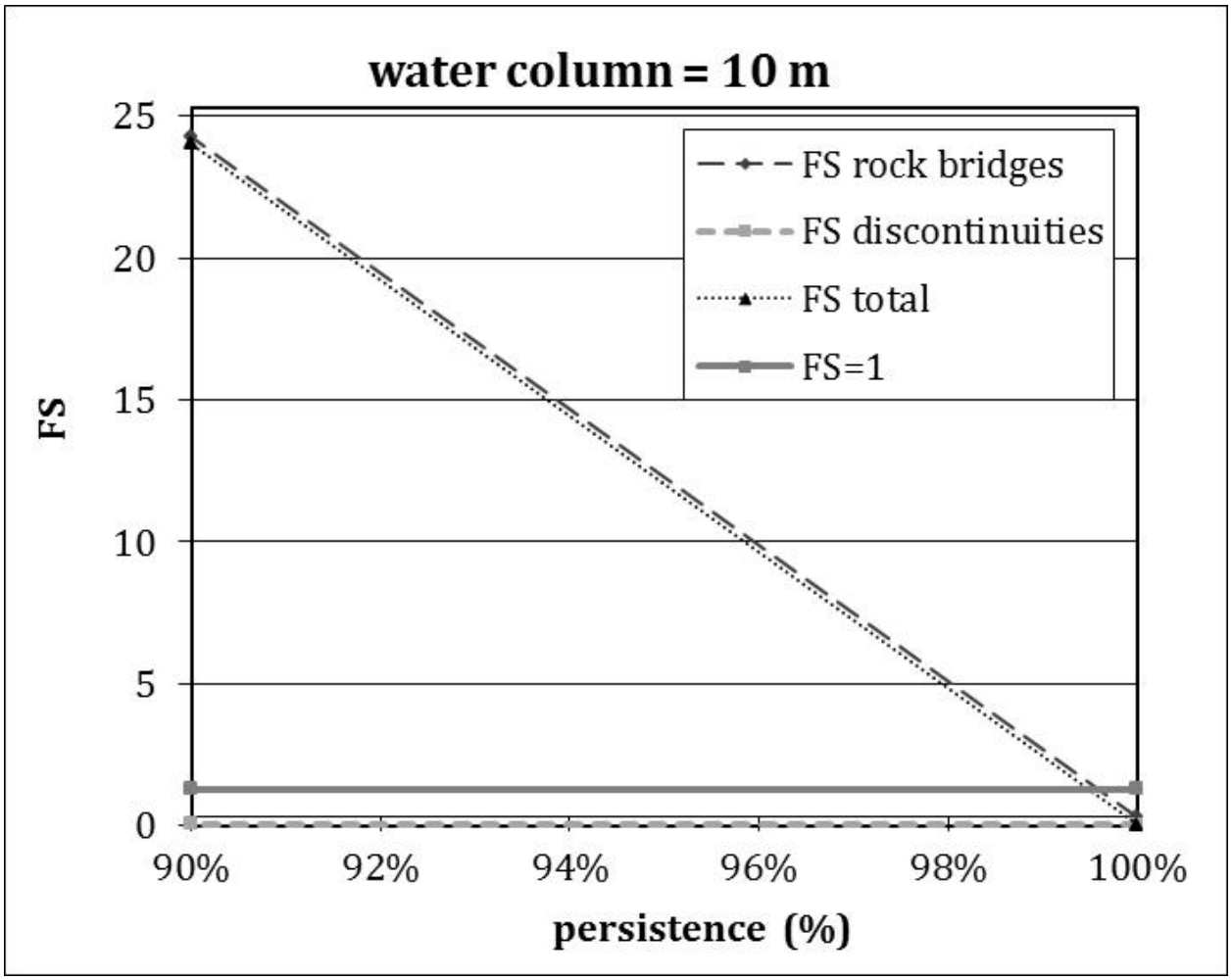

Figure 13. Safety Factor as a function of persistence with the absence of the water column (a) and for a height of 10 m (b).

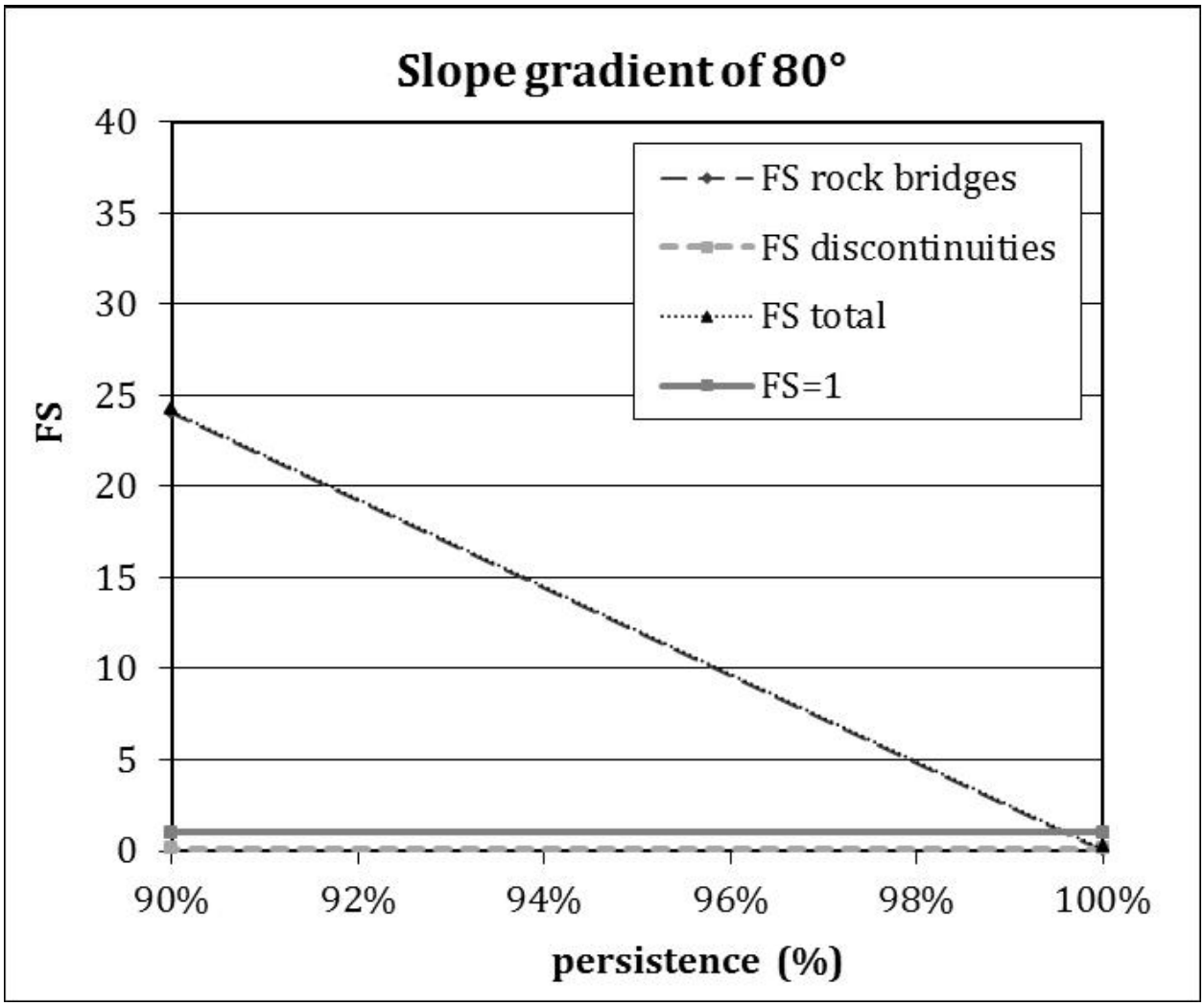

Figure 14. Safety Factor as a function of persistence for a slope inclination of 80° (a) and 40° (b) – no water.

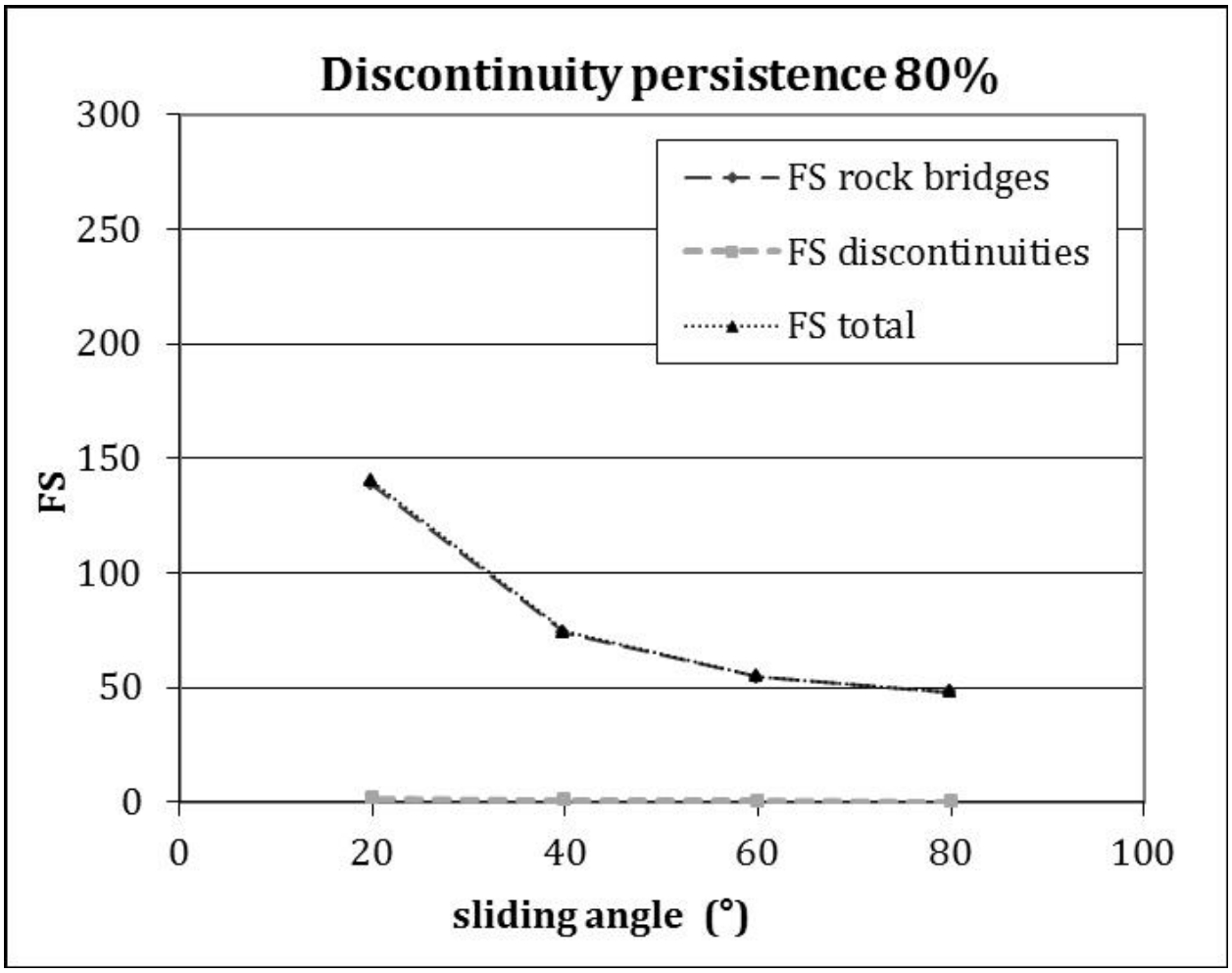

Figure 15. Safety Factor as a function of the sliding angle with a persistence of 80% (a) and 60% (b) – no water.

The results obtained from the parametric analysis show that the temperature increases and the ice melting, introduced in the parametric analyses as an increase in the water level, can induce block instability only if it happens in conjunction with rock bridge failure. This rock bridge failure can indeed be amplified by nocturnal freezing of the water that has reached deeper into the rock fractures during the warmth of the day. These results confirm the assumptions that were based on field observations, although it must be borne in mind that the LEM cannot take into account the condition of progressive failure of rock bridges. This further aspect is analysed in the following section with a DEM.

NUMERICAL MODELLING

The objective of this section is to follow the evolution of block instability using a numerical model. In particular, considering the nature and geometry of the problem to be analysed, the most appropriate numerical model is a distinct element model. 3DEC® software (Itasca, 2012) was used and the methodology consisted of the following steps: creation of the rock mass geometry, definition of the rock matrix and rock discontinuity strengths and application of appropriate boundary conditions.

The overall dimensions of the model were based on the DSM extent (90 m wide and 60 m high) and on the size of the slab that collapsed in September 2007 (15 m wide, 60 m high and 4 m thick). Consequently, the dimensions of the model were taken as: width 50 m, height 60 m and depth 20 m with a slope front inclination of 82° (joint set spacing of 1m). The dimensions were chosen to model a rock mass volume of sufficient size in order to reproduce the instability phenomena whilst avoiding boundary effects. Once the general geometry of the model was complete, all the model blocks were created by applying the joint set orientations reported in Table 1.

The 3DEC input included geometric and mechanical data for each discontinuity set; the software created discontinuities using a random orientation variability of ±2° for each joint set and a spacing of 2.7 m ± 1 m for joint set 1 and 3.1 m ± 2 m for joint set 5. The spacing values and their variability were based on observations from the field survey. The rock blocks were assumed deformable in order to analyse their stability and evolution in detail. As the limit equilibrium evaluations had already been done assuming a rigid block, the progressive failure of the 3DEC deformable blocks captures a different aspect of the stability conditions.

The discontinuity and intact rock strength parameters were the same as those used for the LEM analysis and reported in Table 3. However, only fully persistent joints can be modelled with the 3DEC code and consequently, a fictitious cohesion value of the discontinuity was determined considering the presence of rock bridges that are characterised by rock material strength parameters and considering a joint set persistence of 99%. In this case, cohesion of 0.31 MPa and friction angle of 44° were considered.

The joint deformability features were obtained by considering the Young's modulus of the rock material as an upper limit. In this way, the joint normal stiffness (k_n) was computed directly from Young's modulus of the intact rock, while the shear stiffness (k_s) was determined from consideration of literature data for similar lithology (Giani, 1992); their values were taken as equal to 6.7E+04 and 2.8E+04 MN/m^3, respectively.

The boundary conditions involved the definition of the stresses and the displacements allowed at the model edges. A stress state was applied to the upper model surface to simulate the weight of the upper part of the slope (height 40 m). This stress acted along the vertical direction only. The lower boundary of the model was fixed in the vertical direction. A consolidation phase was initially carried out until convergence was reached and the induced state of stress and displacement was computed.

As the joint network was generated in a random way, the models were run several times for different joint configurations but the same block kinematics was continuously observed. The same kind of block determining the same kind of kinematics was encountered in all simulations and the aim of the model was to evaluate the progressive failure of the slope, as observed in situ. The model showed that the

vertical displacement vectors decreased with slope height and some localised blocks were unstable in the lower part of the slope, as shown in Figure 16. The blocks slid on sub-vertical discontinuities starting from the lower part of the slope and going upwards. This kind of progressive failure mechanism could not be analysed with LEM but corresponds with the observed one.

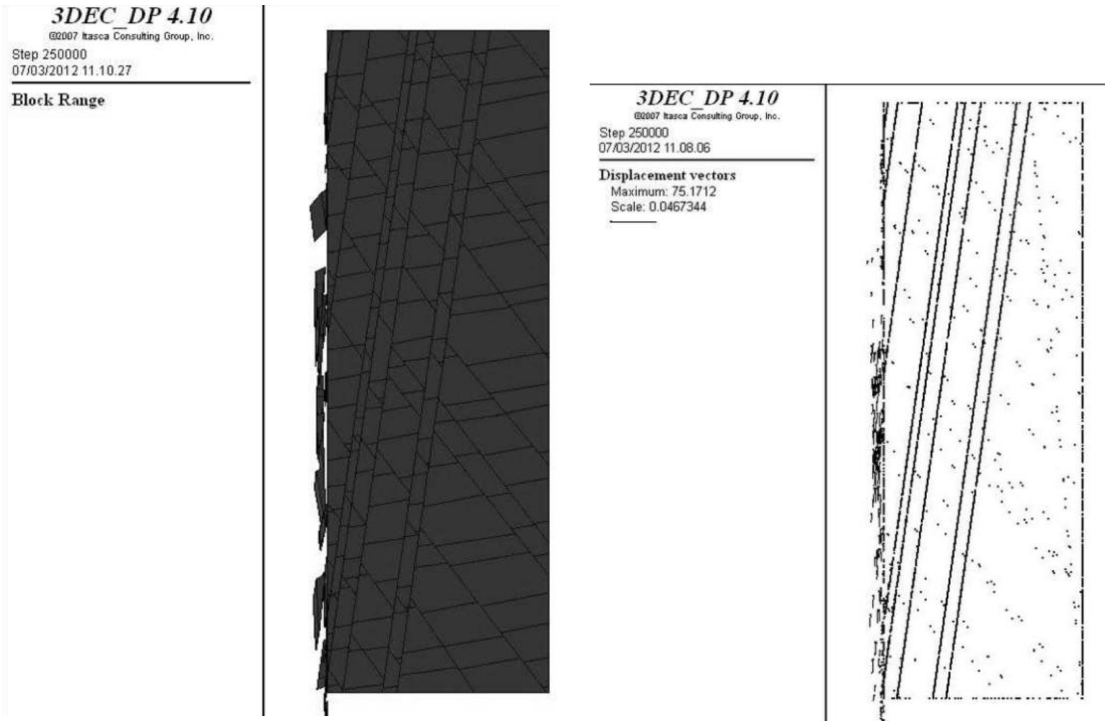

Figure 16. 3DEC unstable blocks (a) and displacement vectors (b) after 250000 calculation cycles. Crop model is 50 m wide, 60 m high and 20 m deep.

The unstable block also showed a similar shape as the one observed in the field, although the volumes of each single block were much smaller; this is also due to the assumption made in the 3DEC code of fully persistent joints in the model. These blocks were bounded by the same discontinuities as they were in the field, which resulted in the same kind of kinematics, identified by the same joint types. However, the volume of each unstable computed block was around 20–25 m^3, similar to the recurrent observed block dimension, while the whole rock block volume involved in the instability phenomenon in 2007 was much larger, estimated at 3600 m^3. This indicates that the 2007 phenomenon could have been governed by a progressive failure due to the movements of several blocks in sequence instead of the falling of one single large monolith.

CONCLUSIONS

Both air and rock temperature data are reported. Air temperature data show that there is both a seasonal and daily variation. At 55 cm depth below the rock surface, the temperature tends to be more constant. During the monitored summer, the air temperature was constantly above 0 °C, while by the end of the summer the air temperature had strong fluctuations that were also recorded in the rock,

reaching values below 0 °C during the night. The rock fall phenomenon occurred in that period of the year, after a long period of high temperatures during which the ice melted and the water circulated into the fracture network. By September, it is realistic to suppose the presence of water inside the discontinuities at greater depths and that the progressive failure of the rock bridges is due to its daily freezing and thawing cycles. However, a measurement of this quantity was not possible, so some parametrical analyses were performed to better understand the failure mechanism.

Parametrical analyses were performed with an LEM analysis, while a DEM analysis was used to better understand the complex, progressive instability phenomenon observed in the field. Both the LEM and the DEM models showed that the blocky rock mass is unstable when rock bridges are absent, even in the absence of water pressures in joints. This result confirms that rock bridges control the actual slope configuration. In the LEM analysis, the study also showed how water can play an important role. The presence of the water assumed in the LEM analysis could be due to ice melting and to the consequent water circulation in the discontinuities, which can change the water pressure regime.

The comparison between the unstable volume and the shape of the blocks computed by DEM, using the rock blocks measured at the base of the slope, has validated the DEM results. However, the volume of a single block in the DEM model was very different from the failed blocks observed at the cliff base, which were determined by the sum of several instability phenomena due to progressive failure. A quantitative comparison of the failed volume is not really possible yet but by continuously monitoring the cliff with periodic surveys, it will be possible to compute the volume of the individual blocks involved in the instability each time it an event occurs. Comparisons between photogrammetric surveys repeated in time will offer useful information on this phenomenon.
The analyses presented in this paper have shown that rises in temperatures and subsequent ice melting, night freezing and consequent rock bridges failure, can induce different water regimes that can strongly influence the stability condition of a slope.

Special consideration should be given to the severe working conditions in environments like the one examined in this paper, which are located at high elevations, involve logistical difficulties in reaching the potentially unstable slopes that are surrounded by glaciers and often only reachable with helicopters. These environmental conditions make field surveys even more complicated and limit the use of certain technologies, such as laser scanners, which involve additional problems (e.g., the equipment is much heavier, usually requires additional batteries or an external electrical generator to ensure sufficient operational time and it must be positioned steadily, etc.) compared with close-range photogrammetry. The proposed method can lead to a better characterisation of this complex situation by providing a more consistent and reliable dataset for the analysis.

Furthermore, the paper shows that for rock fall events, it is important to reconstruct the pre- and post-event conditions using photogrammetric surveys at different times and comparing the obtained DSMs. In this way, it would be possible to determine the mobilised volumes and most importantly, the detachment mechanisms, in order to assess the stability conditions and the potential triggering mechanisms.

Thus, photogrammetric surveys can play two different roles in slope stability investigations: as a surveying tool in the rock mass characterisation at the beginning of the study and as monitoring instrumentation to document the evolution of slope instabilities over time.

ACKNOWLEDGEMENTS

Part of the work was done during the Fondazione Montagna Sicura "CENSI_CRO Monitoraggio dei crolli in roccia in alta quota" project financed by the Council Office for Public Works, Soil Protection and Public House Building, Department for Soil Protection and Water Resources (Eng. R. Rocco, coordinator; Dr. Massimo Broccolato) of the Autonomous Region of the Aosta Valley and thanks to a research scholarship financed by the European Social Fund.

The authors would also like to thank Dr. M. Vagliasindi for his constant support in all the phases of the work.

BIBLIOGRAPHY

Allen S K, Gruber S, Owens I F (2009) Exploring steep bedrock permafrost and its relationship with recent slope failures in the Southern Alps of New Zealand Permafrost and Periglac. Process. 20: 345–356.

Barla G, Dutto F, Mortara G (2000) Brenva glacier rock avalanche of 18 January 1997 on the Mount Blanc range, northwest Italy, Landslide News, 13, 2–5.

Barton, N R (1972) A model study of rock-joint deformation, Int. J. Rock Mech. Min. Sci., 9: 579-602.

CENSI_CRO (2009) Censimento dei Crolli in Roccia in alta quota. *Relazione tecnica finale* Ing. Michèle Curtaz. Available on line, in Italian.

Davies M C R, Hamza O, Harris C (2001) The effect of rise in mean annual temperature on the stability of rock slopes containing ice-filled discontinuities Permafrost Periglac. Process. 12: 137–144

Dutto F, and Mortara G (1991) Grandi frane storiche con percorso su ghiacciaio in Valle d'Aosta, Rev. Valdotaine Hist. Nat., 45, 21– 35.

Dramis F, Govi M, Guglielmin M, and Mortara G (1995) Mountain permafrost and slope instability in the Italian Alps: The Val Pola landslide, Permafrost Periglacial Processes, 6(1), 73– 82.

Deline P (2001) Recent Brenva rock avalanches (Valley of Aosta): New chapter in an old story?, Suppl. Geogr. Fis. Dinam. Quat., 55–63.

Ferrero, A.M., Segalini, A., Giani, G.P. (2010). Stability Analysis of Historic Underground Quarries. Computers and Geotechnics 37 (4) , pp. 476-486

Ferrero A M, Migliazza M, Roncella R, Segalini A (2011) Rock cliffs hazard analysis based on remote geostructural surveys: The Campione del Garda case study (Lake Garda, Northern Italy). Geomorphology 125 (4) , pp. 457-471.

Ferrero A M, Migliazza M, Roncella R and Rabbi E (2011) Rock slopes risk assessment based on advanced techniques. Landslide Vol. 8, N. 2 pag. 221-231 ISSN: 1612-510.

Ferrero A M, Umili G. (2011) Estimating the intensity of rock discontinuities on the base of non-contact survey: application to Aiguille Marbrée (Mont Blanc). International Journal of Rock Mechanics. Vol 48, N.8, pag 1262-1270.

Forlani G, Pinto L (2007) GPS-assisted adjustment of terrestrial blocks. Proc. of the 5th Int. Symp. on Mobile Mapping Technology (MMT'07). Padova, 29-31 maggio 2007, ISSN 1682-1777, CD-ROM

Gigli G, Casagli N (2011) Semi-automatic extraction of rock mass structural data from high resolution LIDAR point clouds. Int. Journal of Rock mechanics 48: 187-198.

Giani G P (1992) Rock slope stability analysis. Balkema, Rotterdam.

Gruber S, Haeberli W (2007) Permafrost in steep bedrock slopes and its temperature-related destabilization following climate change. Journal of Geophysical Research 112: F02S18, doi:10.1029/2006JF000547.

Grün A (1985) Adaptive least squares correlation - a powerful image matching technique. South African Journal of Photogrammetry, Remote Sensing and Cartography, 14 (3), 175-187.

Grün A, Baltsavias E P (1988) Geometrically constrained multiphoto matching. PERS, vol. 54, no. 5, pp 663-671.

Günzel F K (2009) Shear strength of ice-filled rock joints. Ninth International Conference on Permafrost, Alaska

Haeberli W, Huggel C, Kääb A, Polkvoj A, Zotikov I and Osokin N (2003) Permafrost conditions in the starting zone of the Kolka-Karmadon rock/ice slide of 20 September 2002 in North Osetia (Russian Caucasus), paper presented at 8th International Conference on Permafrost, Int. Permafrost Assoc., Zurich, Switzerland.

Hallet B, Walder J S, Stubbs C W (1991) Weathering by segregation ice growth in microcracks at sustained subzero temperatures: Verification from an experimental study using acoustic emissions. Permafrost and Periglacial Processes 2(4). 283–300.

Harrison J P, Reid T R (2000) A semi-automated methodology for discontinuity trace detection in digital images of rock mass exposures. International Journal of Rock Mechanics & Mining Sciences 37: 1073 – 1089.

Hoek E, Carranza-Torres C, Corkum B (2002) Hoek-Brown Failure Criterion -2002 Edition In: 5th North American Rock Mechanics Symposium, Toronto, Canada pp.267-273.Itasca Consulting Group Inc. (1999). 3DEC User Manual. Minneapolis.

Huggel C. Recent extreme slope failures in glacial environments: effects of thermal perturbation, Quaternary Sci. Rev., 28, 1119– 1130, doi:10.1016/j.quascirev.2008.06.007, 2009.

Intergovernmental Panel on Climate Change (2007) Climate Change 2007: The Physical Science Basis. Contribution of Working Group I to the Fourth Assessment Report of the Intergovernmental Panel on Climate Change. Cambridge: Cambridge University Press.

Itasca, (2012) – 3DEC Reference manual, Minneapolis, Minnesota.

Jaboyedoff M, Couture R, Locat P (2009) Structural analysis of Turtle Mountain (Alberta) using digital elevation model: Toward a progressive failure Geomorphology 103, 5–16.

Kemeny J, Monte J, Handy J, Thiam S (2003) The use of digital imaging and laser scanning technologies in rock engineering. In Int. Symp. n the Fusion Technology of Geosystem Engineering, Rock Engineering and Geophysical Exploration, Seoul, Korea, 18-19 November.

Matsuoka N, Sakai H (1999) Rockfall activity from an alpine cliff during thawing periods. Geomorphology 28(3–4). 309–328.

Murton J B, Coutard J-P, Lautridou J-P, Ozouf J-C, Robinson D A and Williams R B G (2001) Permafrost And Periglacial Processes, Permafrost Periglac. Process. **12**: 255–266

Noetzli J, Hoelzle M and Haeberli W (2003) Mountain permafrost and recent Alpine rock-fall events: A GIS-based approach to determine critical factors, paper presented at 8th International Conference on Permafrost, Int. Permafrost Assoc., Zurich, Switzerland.

Palmstrom A, Singh R (2001) The deformation modulus of rock masses: comparison between in situ tests and indirect estimates. Tunnelling and Underground Space Technologies. 16: 115-31.

Ravanel L, Deline P (2011) Climate influence on rockfalls in high-alpine steep rockwalls: The north side of the Aiguilles de Chamonix (Mont Blanc massif) since the end of the 'Little Ice Age'. The Holocene 21: 357-365.

Ryzhkin I, Petrenko V (1997) Physical mechanisms responsible for ice adhesion. J. Physical Chem. B 101 (32), 6267-6270.

Rocscience Inc. (2009) DIPS, Toronto, Canada.

Rocscience Inc. (2007) RocData 4.0 Guide. Toronto, Canada.

Roncella R, Forlani G, Remondino F (2005) Photogrammetry for geological applications: automatic retrieval of discontinuity orientation in rock slopes. In Videometrics IX – Eletronic Imaging – IS&T/SPIE 17th Annual Symposium, 17-27.

Sturzenegger M, Stead D (2009a) Quantifying discontinuity orientation and persistence on high mountain rock slopes and large landslides using terrestrial remote sensing techniques. Natural Hazards and Earth System Science9: 267–87.

Sturzenegger M, Stead D (2009b) Close-range terrestrial digital photogrammetry and terrestrial laser scanning for discontinuity characterization on rock cuts. Engineering Geology106:163–82.

Suter S (2002) Cold firn and ice in the Monte Rosa and Mont Blanc areas: Spatial occurrence, surface energy balance and climate evidence, Ph.D. thesis, Versuchsanst. Wasserbau, Hydrol. und Glaziol., ETH Zurich, Switzerland.

Umili G, Ferrero A, Einstein H H (2012) A new method for automatic discontinuity traces sampling on rock mass 3D model. Computes and geosciences. Available on line.

Vincent C, Le Meur E, Six D, Funk M, Hoelzle M and Preunkert S (2007) Very high-elevation Mont Blanc glaciated areas not affected by the 20th century climate change, J. Geophys. Res., 112, D09120, doi:10.1029/2006JD007407.

Figure 1
Click here to download Figure: figure 1.doc

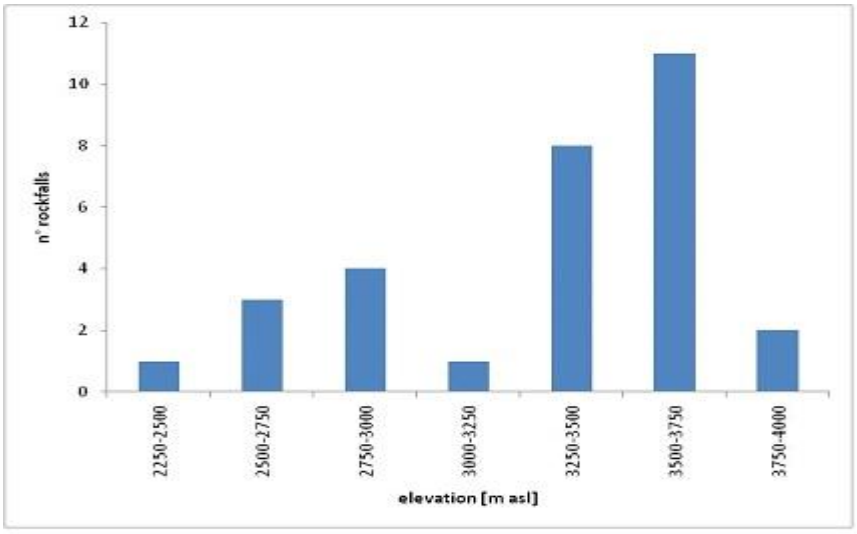

Figure 1 . Rock fall events recoreded in Valle d'Aosta (Italy) between 2006 and 2009 (CENSI CRO final report, 2009).

Figure 2
Click here to download high resolution image

Figure 3
Click here to download high resolution image

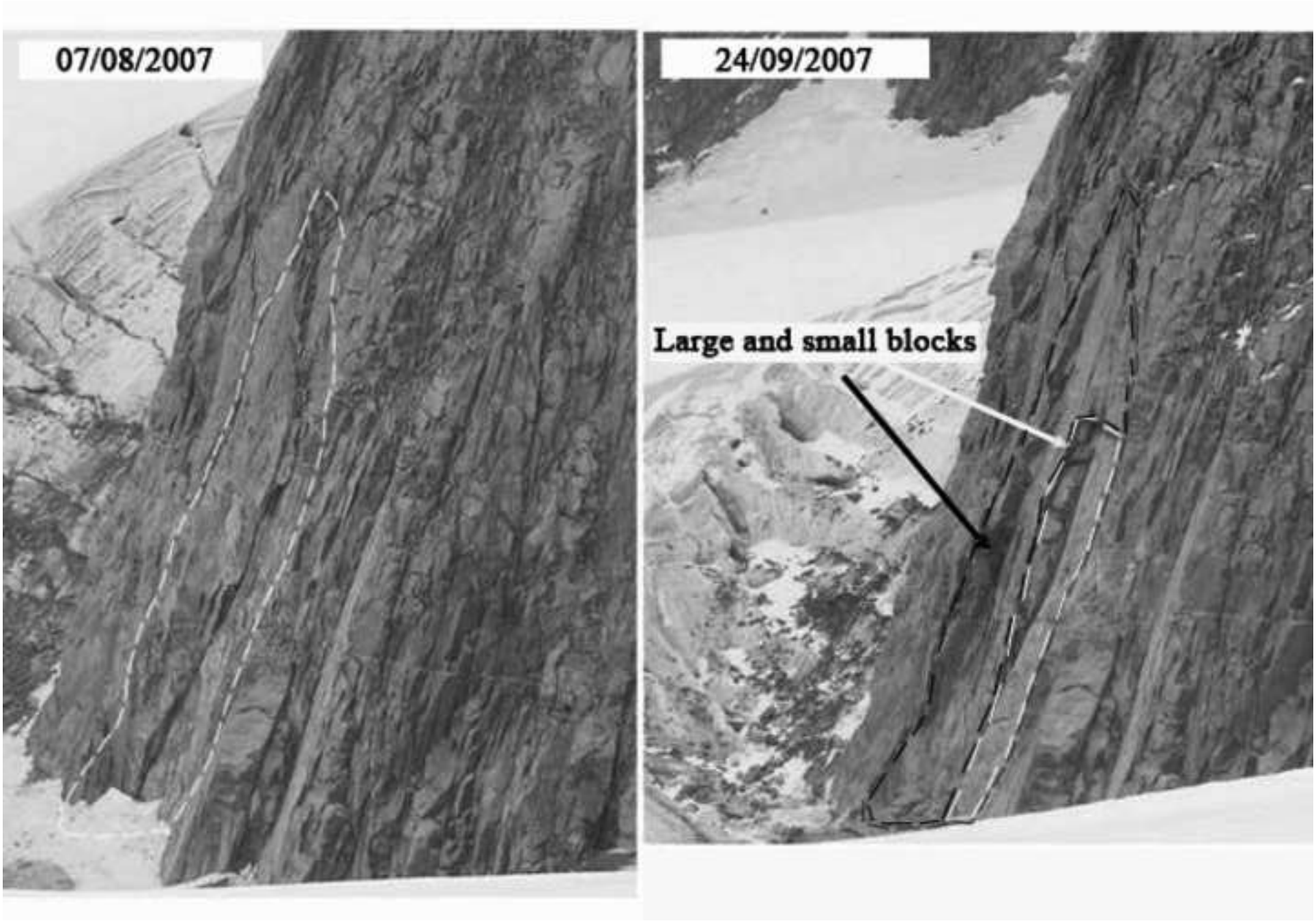

Figure 4
Click here to download Figure: Figure 4.doc

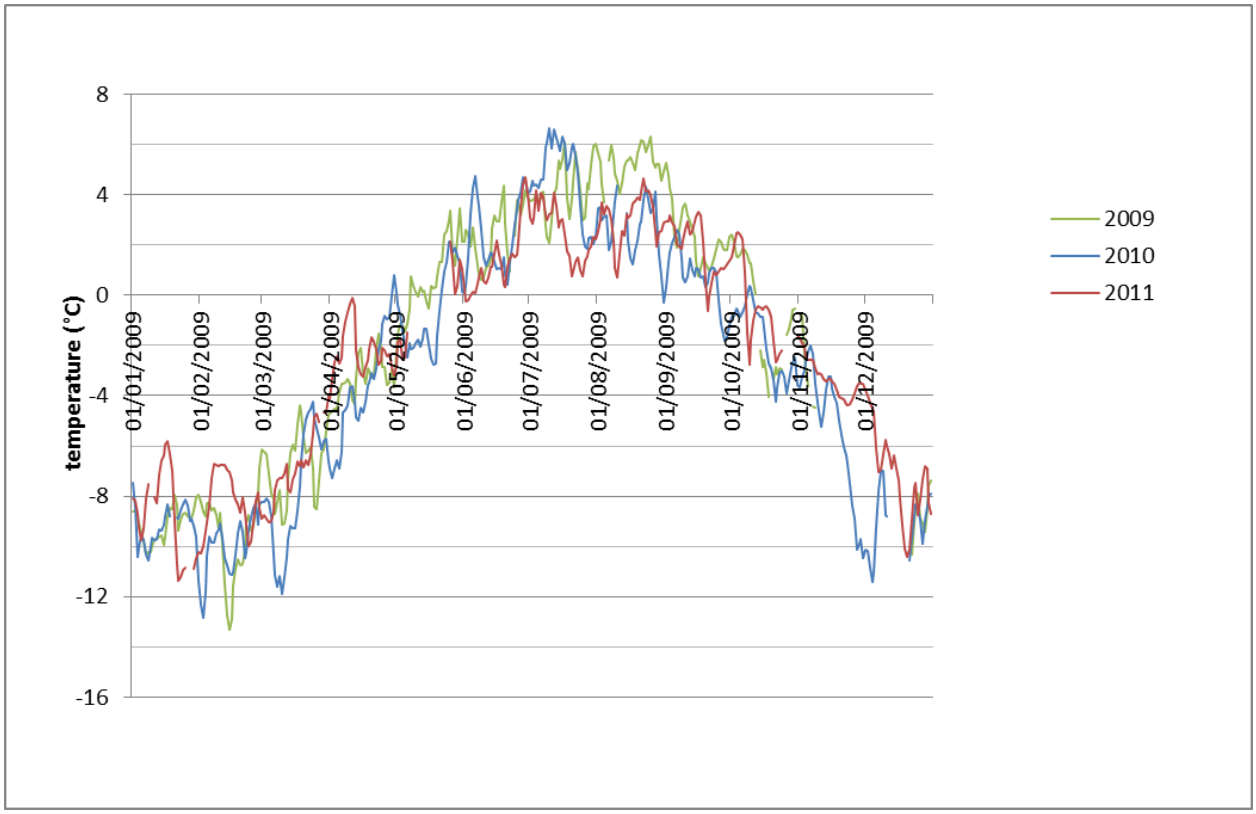

Figure 4. Rock temperature data collected at Punta Helbronner meteo station at 55cm depth.

Figure 5
Click here to download Figure: Figure 5.doc

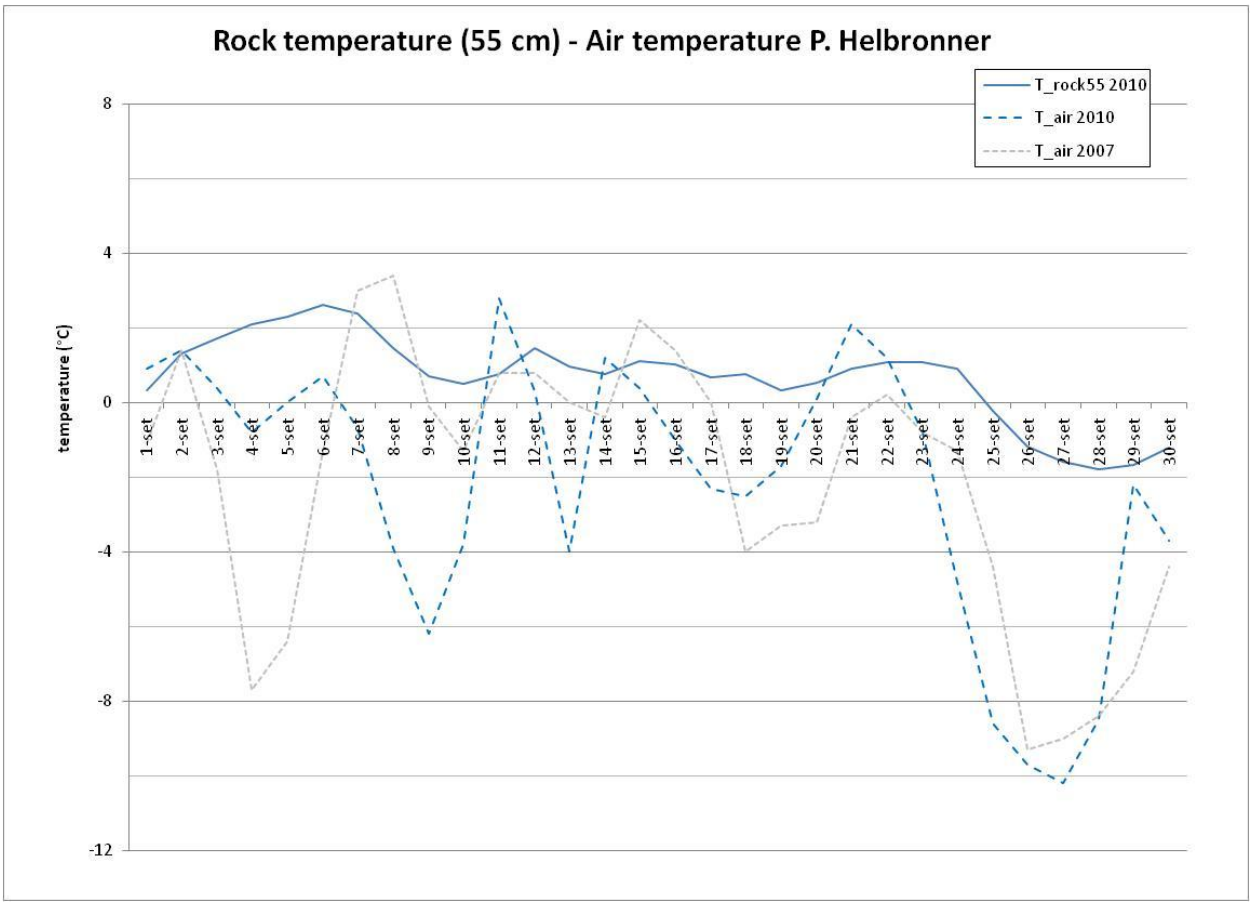

Figure 5. Comparison between rock and air temperature data.

Figure 6
Click here to download high resolution image

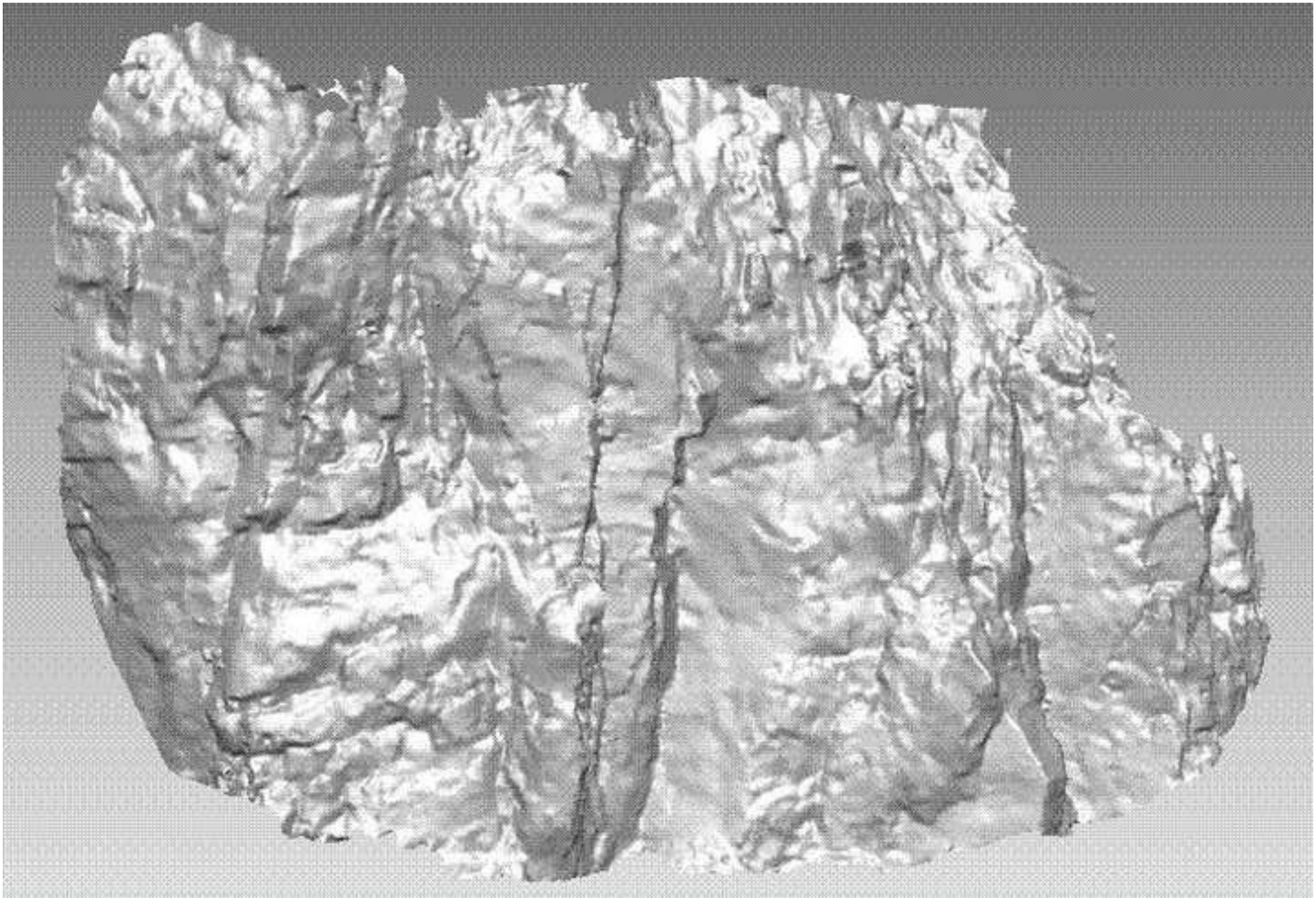

Figure 7
Click here to download high resolution image

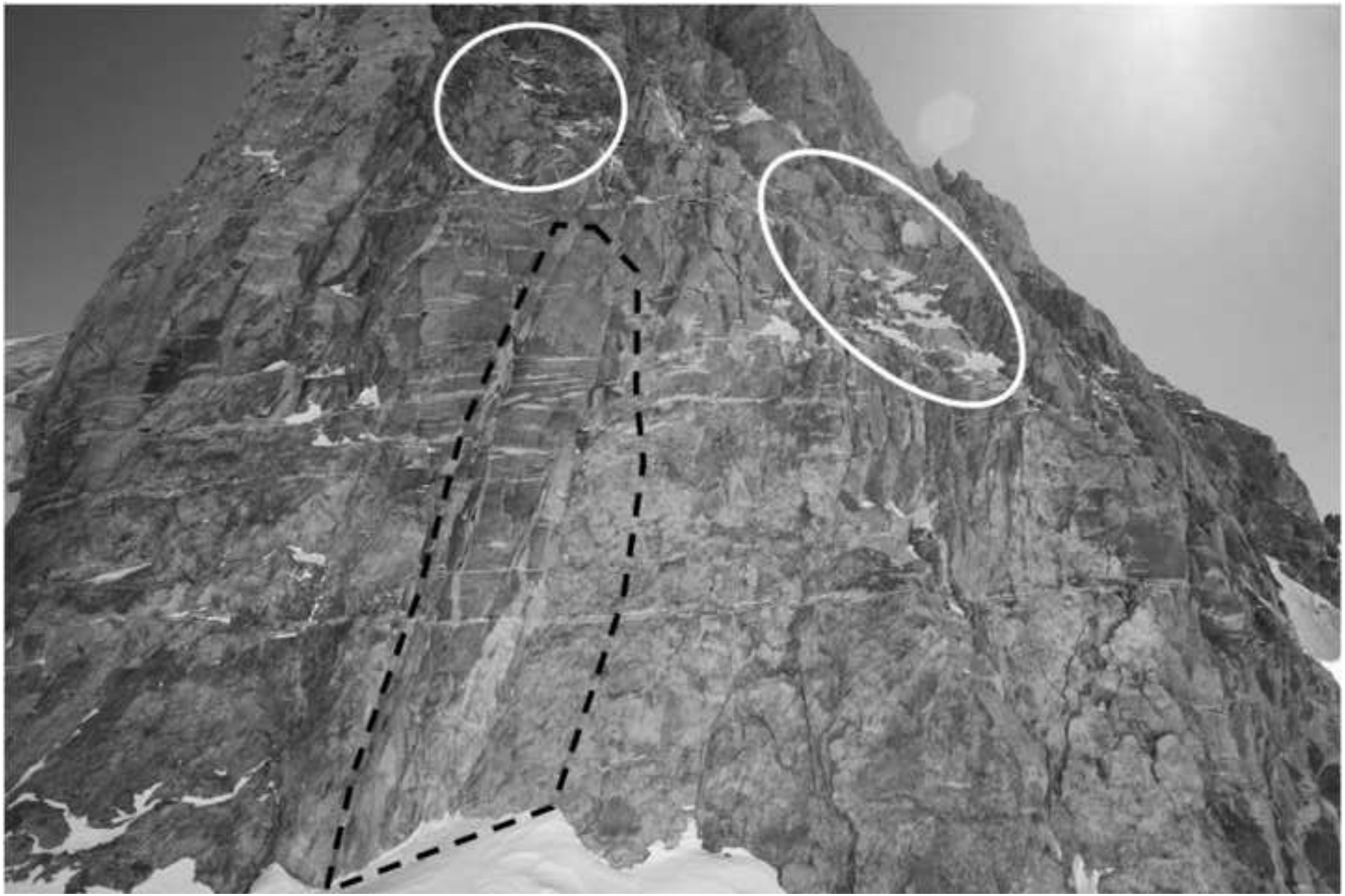

Figure 8
Click here to download high resolution image

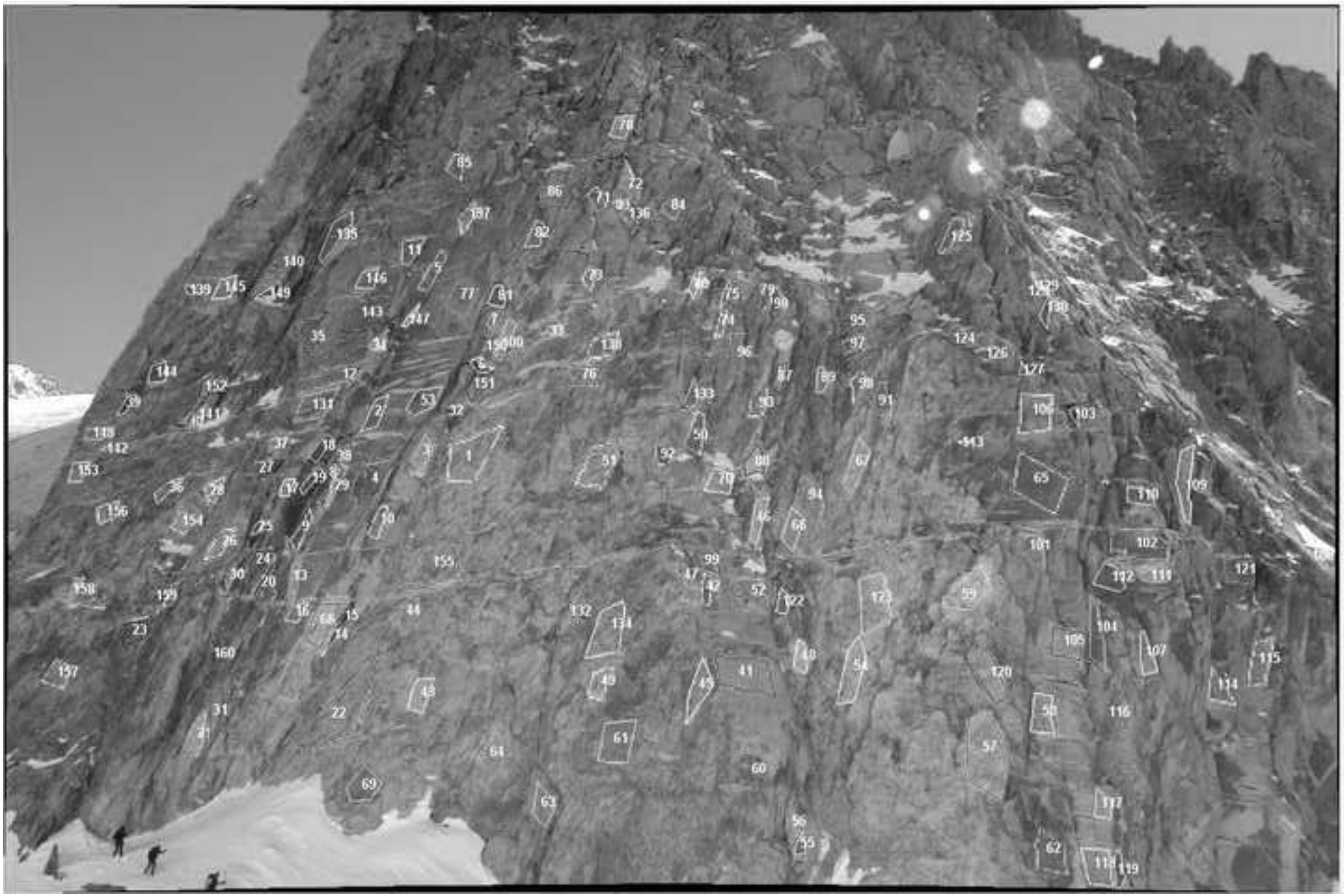

Figure 9
Click here to download high resolution image

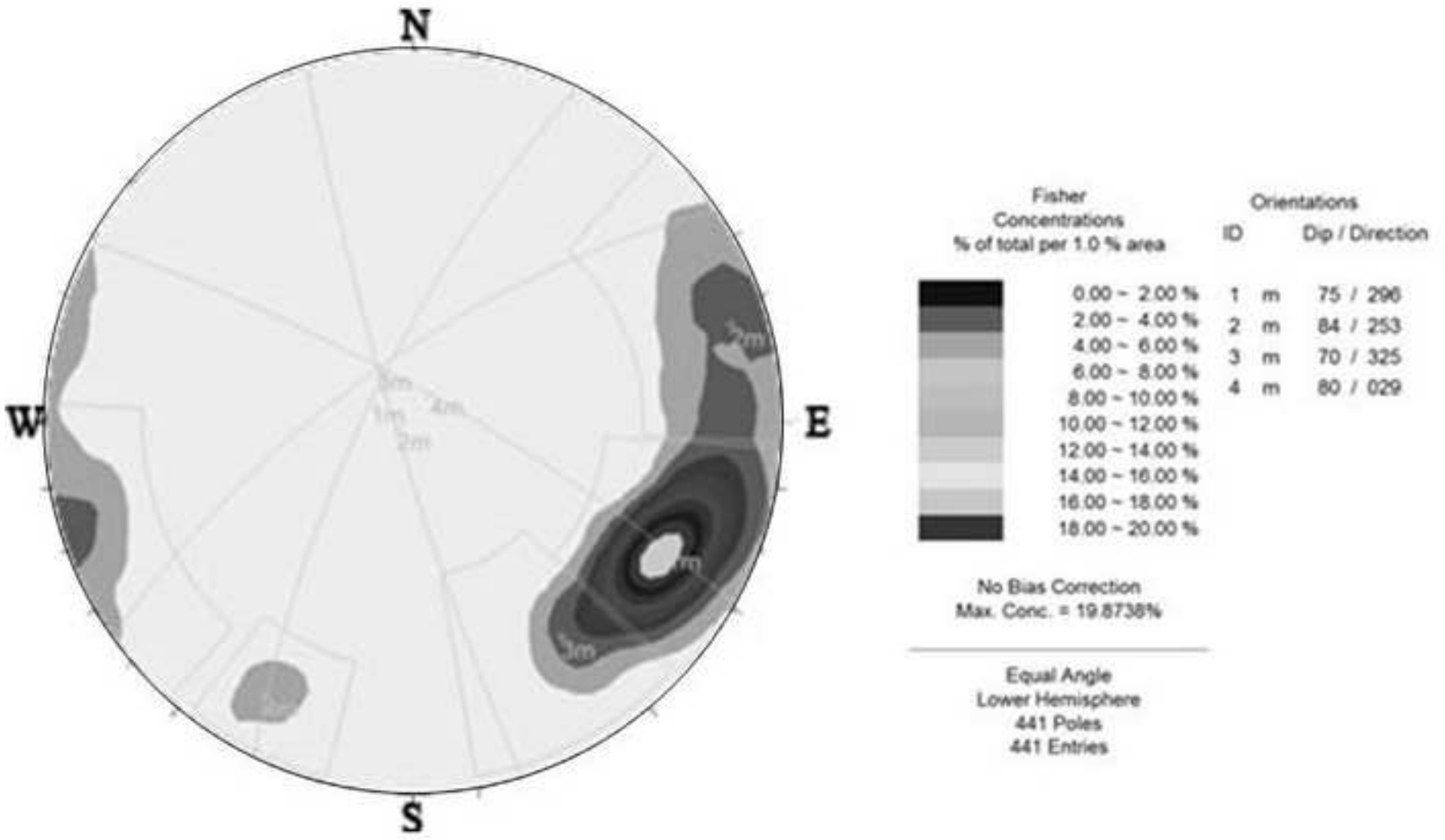

Figure 10
Click here to download high resolution image

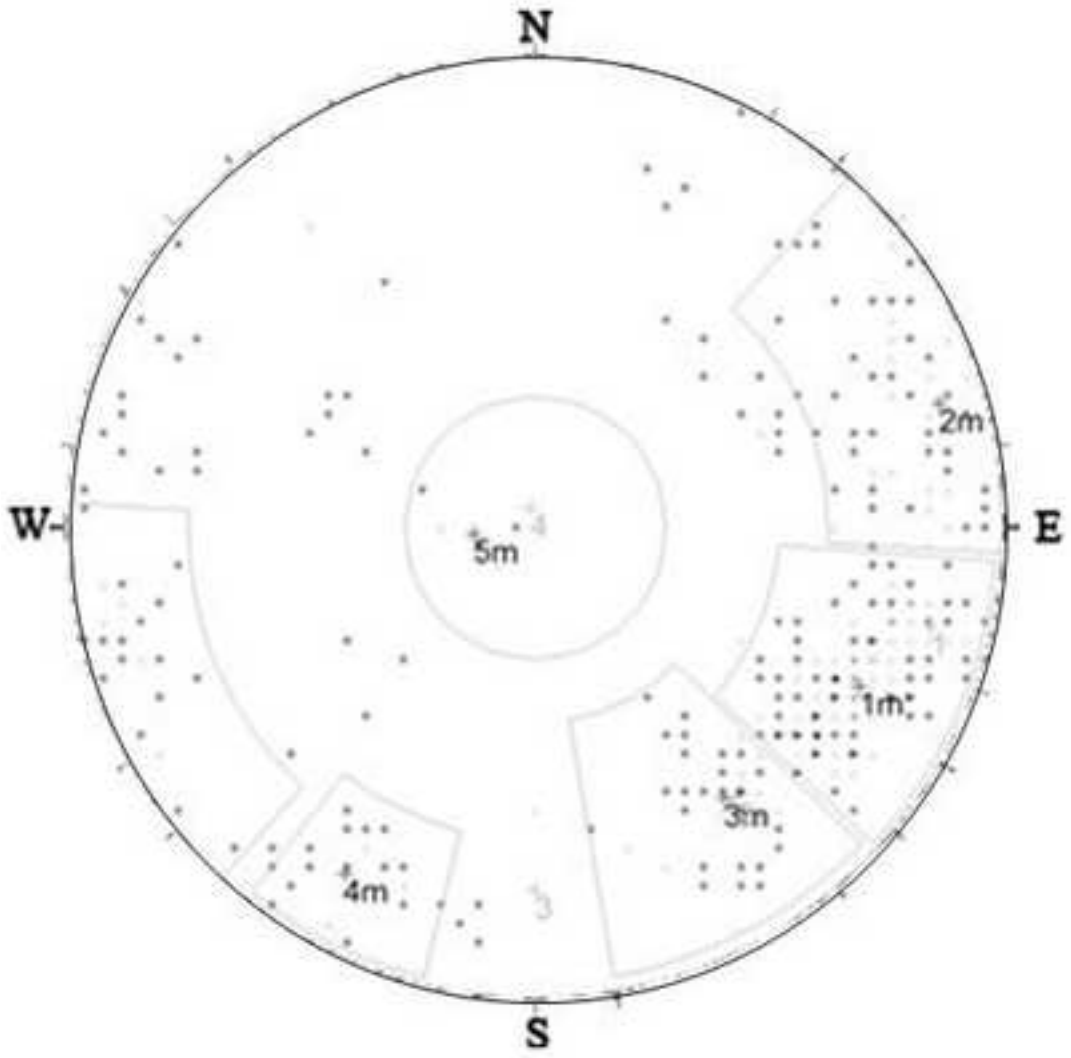

Number of Poles

- 1 pole
- 2 to 3 poles
- 4 to 5 poles
- 6 to 7 poles
- 8 to 9 poles
- 10 to 11 poles

Equal Angle
Lower Hemisphere
441 Poles
441 Entries

Orientations

ID		Dip / Direction
1		82 / 284
2		71 / 323
3		75 / 360
4		05 / 166
1	m	75 / 296
2	m	84 / 253
3	m	70 / 325
4	m	80 / 029
5	m	15 / 084

Figure 11
Click here to download high resolution image

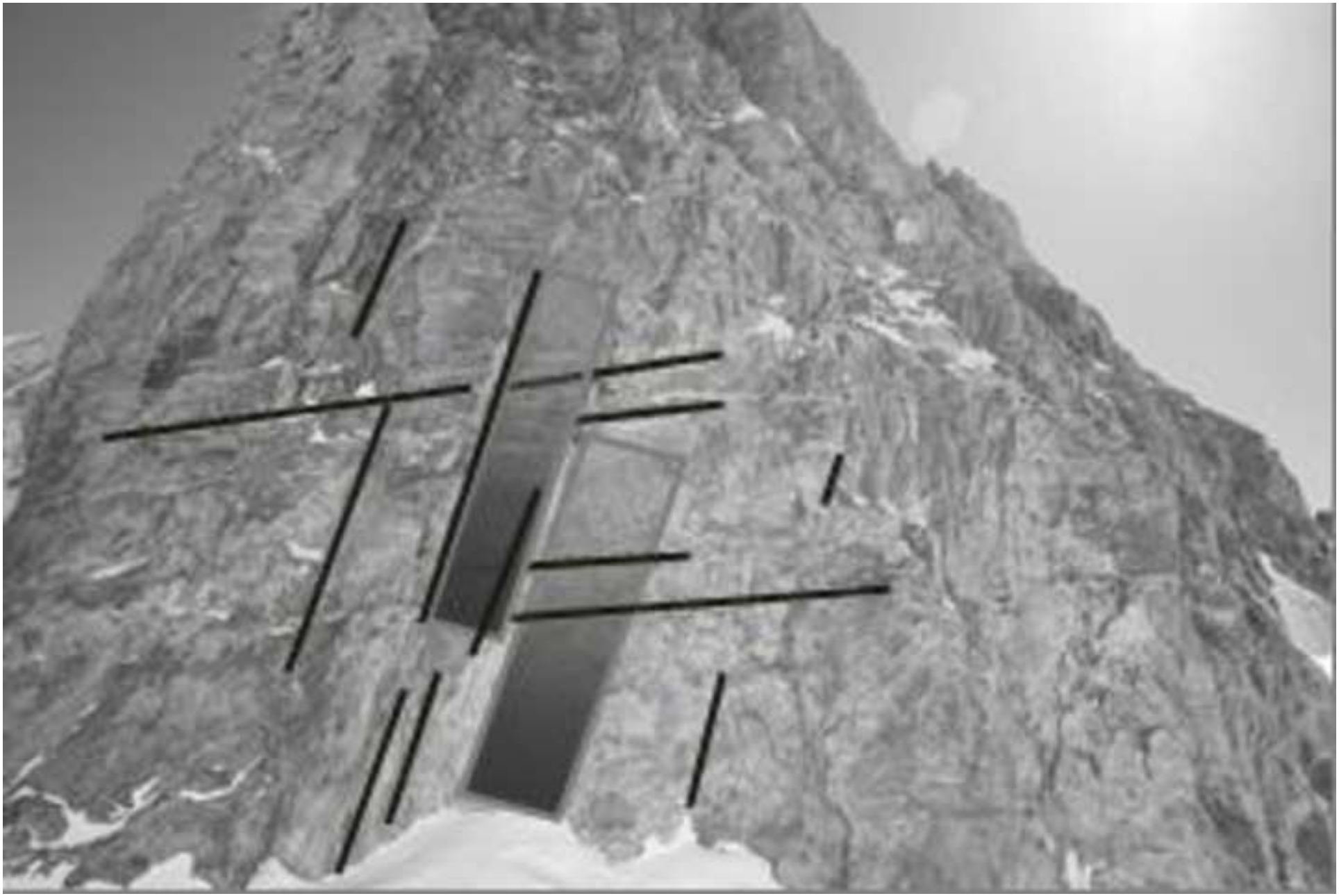

Figure 12
Click here to download high resolution image

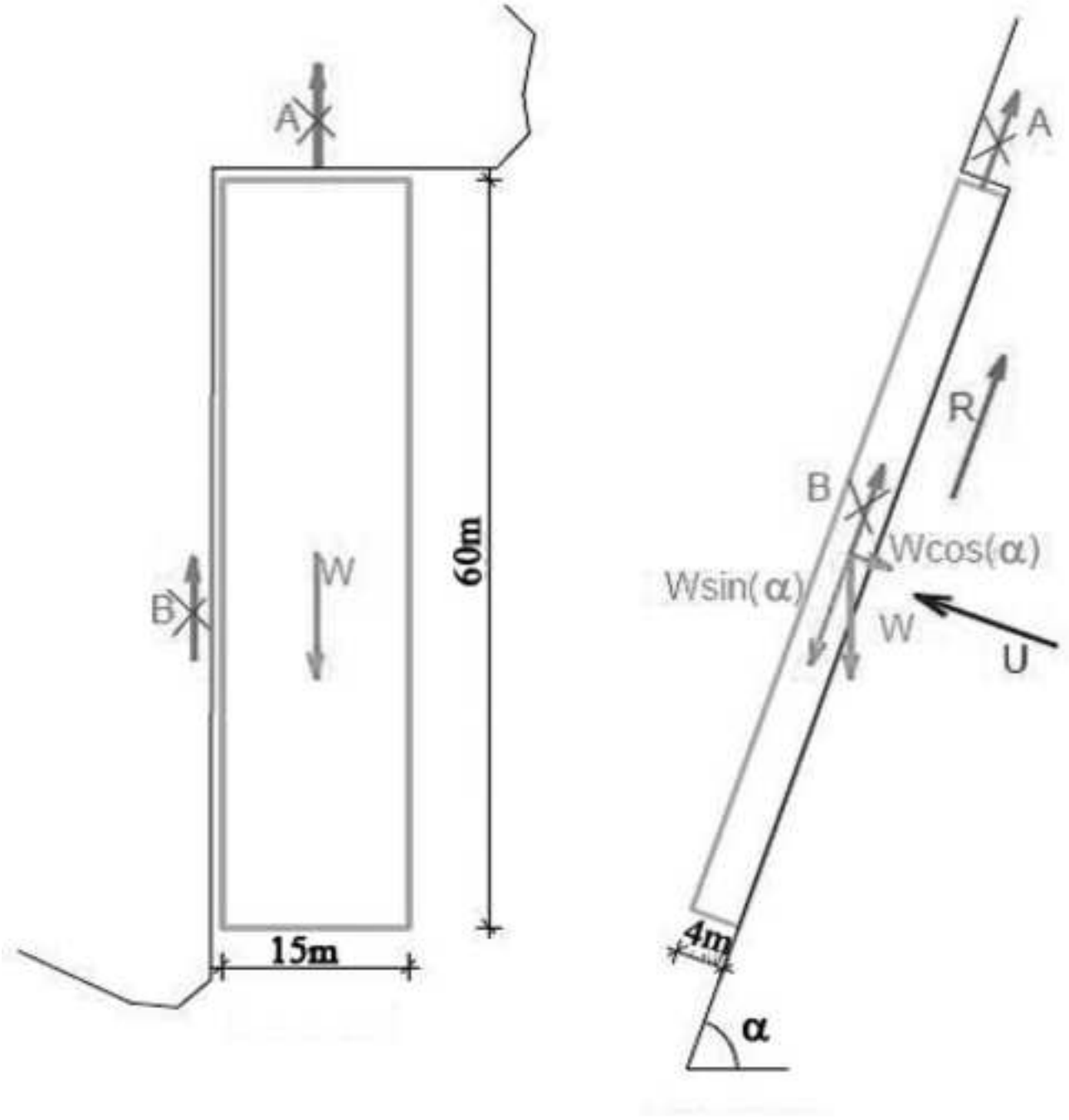

Figure 13
Click here to download high resolution image

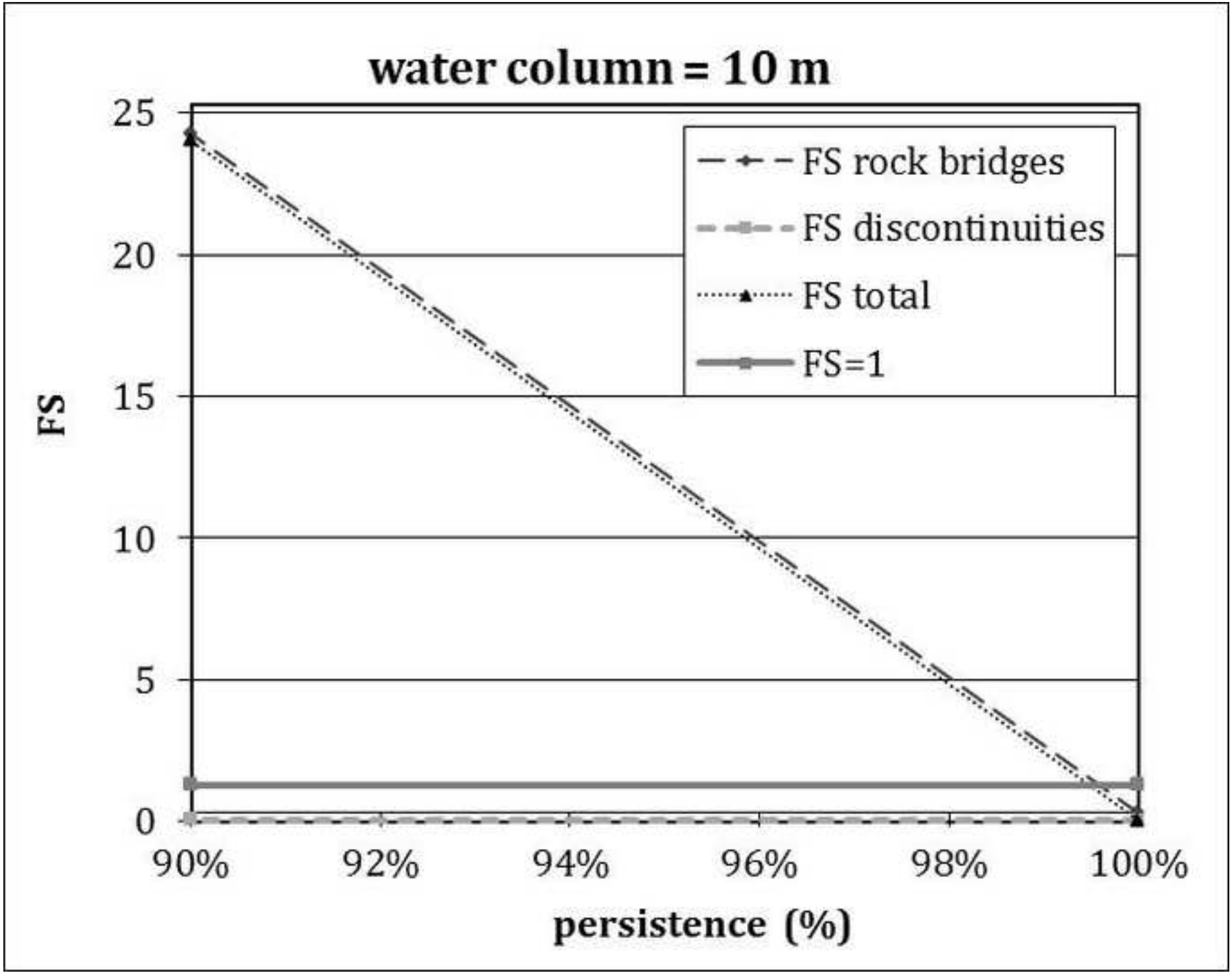

Figure 14
Click here to download high resolution image

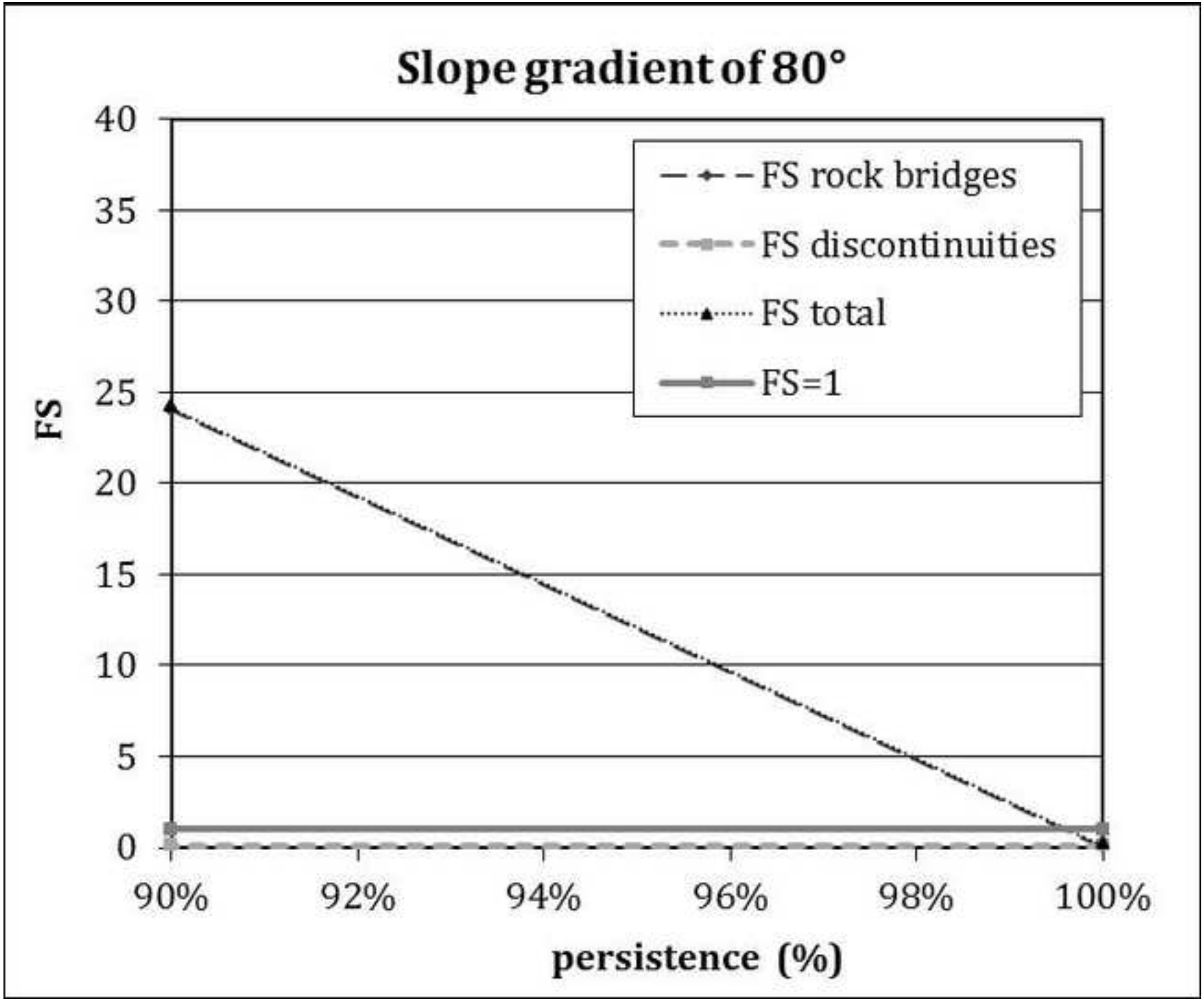

Figure 15
Click here to download high resolution image

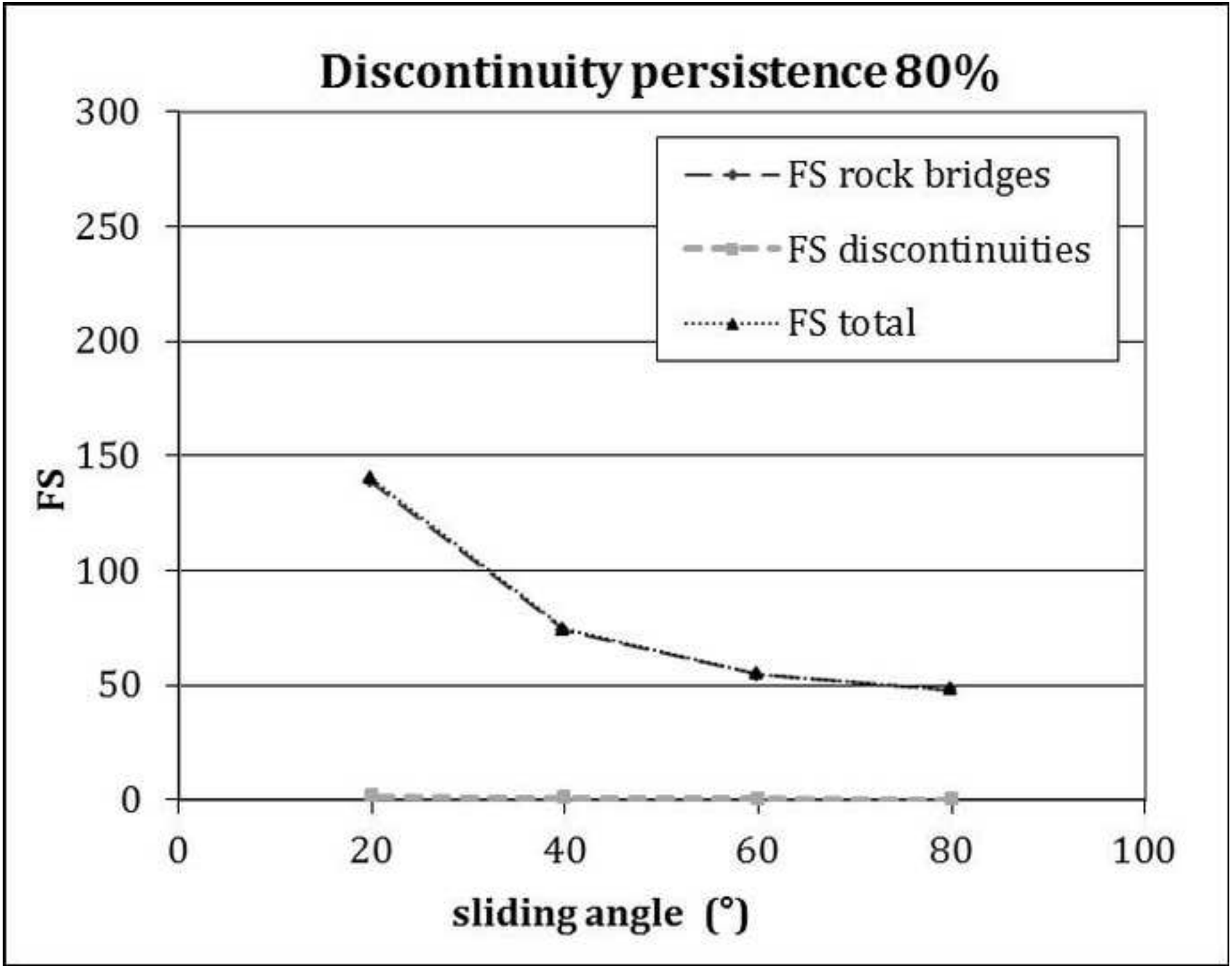

Figure 16
Click here to download Figure: Figure 16.doc

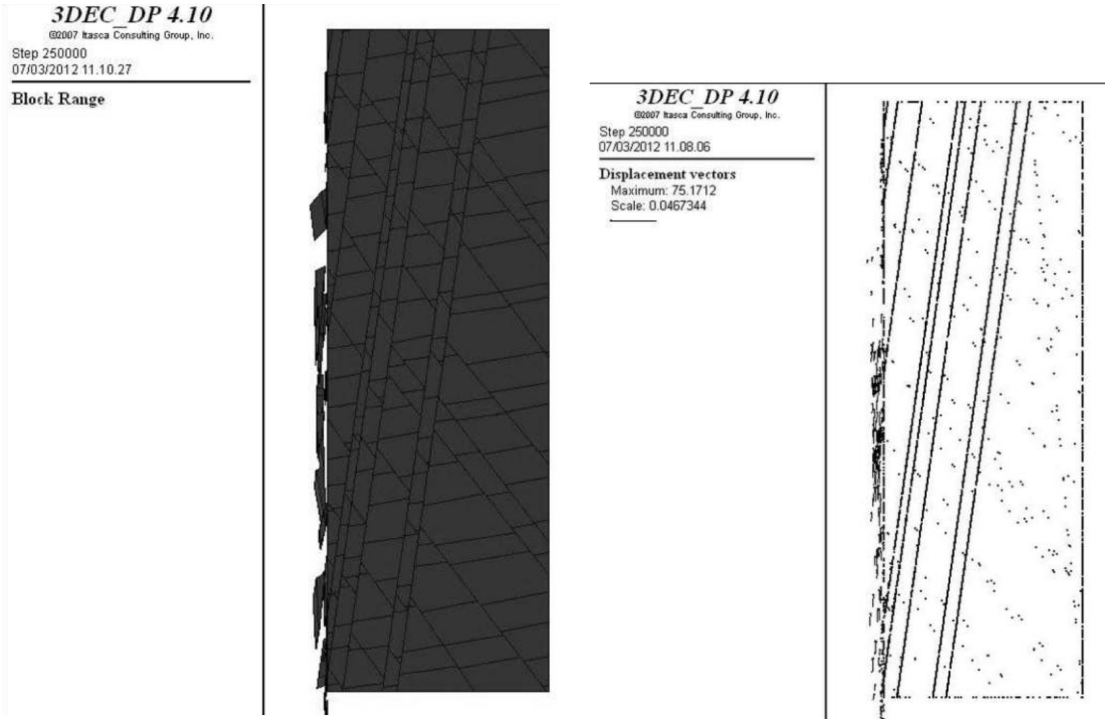

Figure 16. 3DEC unstable blocks (a) and displacement vectors (b) after 250000 calculation cycles. Crop model is 50 m wide, 60 m high and 20 m deep.

Table 1
Click here to download Table: Table 1.doc

Discontinuity set	**Traditional survey**	**Rockscan survey**	**Differences**
Parallel to the cliff face	82/284 (1)	75/296 (1m)	7 / 12
Lateral release	75/000 (3)	80/029 (4m)	5 / 29
Sub-horizontal	05/166 (4)	15/084 (5m)	10 / 82
Other	71/323 (2)	70/325 (3m)	1 / 2

Table 1. Mean orientation values and differences obtained with Rockscan and with the traditional survey. The ID discontinuity set is shown in parentheses.

Table 2
Click here to download Table: Table 2.doc

Table 1: Geometry.

L_a	Block dimension	15 m
L_b	Block dimension	60 m
L_c	Block dimension	4 m
V	Block volume	3600 m^3
$S = L_a \cdot L_b$	Sliding surface	900 m^2
α	Sliding surface angle	80 °

Table 3
Click here to download Table: Table 3.doc

Table 1: Rock bridge and joint parameters.

γ	Specific weight	2.7 kg/dm^3
φ_j	Joint friction angle	35 °
c_j	Joint cohesion	0 MPa
φ_r	Rock bridge friction angle	46 °
c_r	Rock bridge cohesion	25 MPa